

Normal and lateral Casimir force: Advances and prospects

G. L. Klimchitskaya

Department of Physics, North-West Technical University, Millionnaya Street 5, St.Petersburg, 191065, Russia

and

Institute for Theoretical Physics, Leipzig University, Postfach 100920, D-04009, Leipzig, Germany

E-mail: galina.klimchitskaya@itp.uni-leipzig.de

Abstract. We discuss recent experimental and theoretical results on the Casimir force between real material bodies made of different materials. Special attention is paid to calculations of the normal Casimir force acting perpendicular to the surface with the help of the Lifshitz theory taking into account the role of free charge carriers. Theoretical results for the thermal Casimir force acting between metallic, dielectric and semiconductor materials are presented and compared with available experimental data. Main attention is concentrated on the possibility to control the magnitude and sign of the Casimir force for applications in nanotechnology. In this respect we consider experiments on the optical modulation of the Casimir force between metal and semiconductor test bodies with laser light. Another option is the use of ferromagnetic materials, specifically, ferromagnetic dielectrics. Under some conditions this allows to get Casimir repulsion. The lateral Casimir force acting between sinusoidally corrugated surfaces can be considered as some kind of noncontact friction caused by zero-point oscillations of the electromagnetic field. Recent experiments and computations using the exact theory have demonstrated the role of diffraction-type effects in this phenomenon and the possibility to get asymmetric force profiles. Conclusion is made that the Casimir force may play important role in the operation of different devices on the nanoscale.

1. Introduction

Both the van der Waals and Casimir forces are quantum phenomena originating from the interaction of electromagnetic fluctuations with matter. One difference between them is that the van der Waals force is nonrelativistic, whereas the Casimir force takes full account of the relativistic retardation effects. Thus, in fact there exists just one force of a fluctuation nature. At shortest separations up to a few nanometers between the interacting bodies, where retardation is negligibly small, it is referred to as the *van der Waals* force. At larger separations it is called the *Casimir* force [1].

The Casimir force becomes significantly large if measured at separations below one micrometer. At separations below 100 nm it competes with characteristic electric forces acting between the constituting elements of microelectromechanical and nanoelectromechanical devices. The attractive Casimir force leads to pull-in and stiction [2] which may result in the collapse of a microdevice. That is why the Casimir force has attracted much recent attention in nanotechnology. On the one hand, it can be used as an actuating force [3] in place of electric

forces. On the other hand, it plays the role of some kind friction in micrometer scales which cannot be diminished by means of lubrication. In this respect, the possibility of repulsive Casimir force attracts much public attention as the mean to cancel this friction.

It is commonly known that the unified description of both the van der Waals and Casimir forces is given by the Lifshitz theory [4, 5]. During more than forty years after this theory was created it was lacking detailed experimental confirmation due to the absence of sufficiently precise measurements. During the last decade, however, many experiments measuring the Casimir force have been performed (see the recent review [6]). The comparison between the measurement data of the most precise experiments and computational results on the basis of the Lifshitz theory has led to a puzzle. It turned out that the Lifshitz theory is in agreement with the data only under a condition that for metallic test bodies the relaxation properties of conduction electrons are not accounted for, whereas for dielectrics charge carriers are completely discarded (controversial discussions concerning these results are reflected in Ref. [7]). Modern overview of both experimental and theoretical aspects of the Casimir force can be found in the monograph [8].

The present paper reviews several recent experimental and theoretical results in the Casimir effect which are of much importance for understanding of delicate physical mechanisms of fluctuation-induced forces and for their technological application in new generations of micro- and nanoelectromechanical systems. In Sec. 2 we briefly discuss the standard formalism of the Lifshitz theory, its generalization for the case of nonplanar geometries, and modifications aimed to resolve the above-mentioned puzzle. Section 3 is devoted to the comparison of theoretical results with the experimental data of three landmark experiments. These experiments were performed with metallic [9, 10, 11, 12], semiconductor [13, 14], and dielectric [15, 16] test bodies. In Sec. 4 the possibilities to control the magnitude and sign of the Casimir force by using materials with different electric and magnetic properties are considered. These include the variation of the density of free charge carriers with laser light, the use of three-layer systems and phase transitions, investigation of the Casimir force between ferromagnetic dielectrics etc. Special attention is devoted in Sec. 5 to the lateral Casimir force arising between sinusoidally corrugated surfaces, as predicted theoretically in Ref. [17] and experimentally demonstrated in Refs. [18, 19]. It was shown quite recently [20, 21] that this phenomenon has potential for applications in nanotechnology. Our conclusions and discussion are contained in Sec. 6.

2. Brief formulation of the Lifshitz theory

The Lifshitz theory [4, 5] expresses the free energy and pressure of the van der Waals and Casimir interaction in the configuration of two parallel semispaces (thick plates) separated with a gap of width a at temperature T in the following form:

$$\mathcal{F}(a, T) = \frac{k_B T}{2\pi} \sum_{l=0}^{\infty} \prime \Phi_E(\xi_l), \quad (1)$$

$$P(a, T) = -\frac{\partial \mathcal{F}(a, T)}{\partial a} = -\frac{k_B T}{\pi} \sum_{l=0}^{\infty} \prime \Phi_P(\xi_l).$$

Here, k_B is the Boltzmann constant, $\xi_l = 2\pi k_B T l / \hbar$ with $l = 0, 1, 2, \dots$ are the Matsubara frequencies, and the terms with $l = 0$ in the primed sums are multiplied by $1/2$. The functions Φ_E and Φ_P are expressed in terms of reflection coefficients on the two semispaces $r_\alpha^{(1)}$ and $r_\alpha^{(2)}$ for two independent polarizations of the electromagnetic field, transverse magnetic ($\alpha = \text{TM}$) and transverse electric ($\alpha = \text{TE}$),

$$\Phi_E(x) = \int_0^\infty k_\perp dk_\perp \sum_\alpha \ln \left[1 - r_\alpha^{(1)}(ix, k_\perp) r_\alpha^{(2)}(ix, k_\perp) e^{-2aq} \right],$$

$$\Phi_P(x) = \int_0^\infty k_\perp dk_\perp q \sum_\alpha \left[\frac{e^{2aq}}{r_\alpha^{(1)}(ix, k_\perp) r_\alpha^{(2)}(ix, k_\perp)} - 1 \right]^{-1}, \quad (2)$$

where

$$q \equiv q(ix, k_\perp) = \sqrt{k_\perp^2 + x^2/c^2}, \quad (3)$$

and $\mathbf{k}_\perp = (k_x, k_y)$ is the projection of a wave vector on the plane of plates. The reflection coefficients on homogeneous media described by the frequency-dependent dielectric permittivity $\varepsilon^{(n)}(\omega)$ and magnetic permeability $\mu^{(n)}(\omega)$ ($n = 1, 2$) are given by

$$r_{\text{TM}}^{(n)}(ix, k_\perp) = \frac{\varepsilon^{(n)}(ix)q - k^{(n)}}{\varepsilon^{(n)}(ix)q + k^{(n)}}, \quad r_{\text{TE}}^{(n)}(ix, k_\perp) = \frac{\mu^{(n)}(ix)q - k^{(n)}}{\mu^{(n)}(ix)q + k^{(n)}}, \quad (4)$$

where

$$k^{(n)} \equiv k^{(n)}(ix, k_\perp) = \sqrt{k_\perp^2 + \varepsilon^{(n)}(ix)\mu^{(n)}(ix)\frac{x^2}{c^2}}. \quad (5)$$

The Lifshitz-type formulas similar to (1) hold also for the Casimir-Polder free energy and force acting between an atom with dynamic electric polarizability $\alpha(\omega)$ and magnetic susceptibility $\beta(\omega)$ and a wall described by $\varepsilon(\omega)$ and $\mu(\omega)$

$$\begin{aligned} \mathcal{F}_A(a, T) &= -k_B T \sum_{l=0}^{\infty}{}' \int_0^\infty k_\perp dk_\perp q_l \Phi_A(\xi_l, k_\perp), \\ F_A(a, T) &= -k_B T \sum_{l=0}^{\infty}{}' \int_0^\infty k_\perp dk_\perp q_l^2 \Phi_A(\xi_l, k_\perp), \end{aligned} \quad (6)$$

where $q_l = q(i\xi_l, k_\perp)$. The function $\Phi_A(\xi_l, k_\perp)$ is defined as [22]

$$\begin{aligned} \Phi_A(x, k_\perp) &= e^{-2aq} \left\{ 2 [\alpha(ix) r_{\text{TM}}(ix, k_\perp) + \beta(ix) r_{\text{TE}}(ix, k_\perp)] \right. \\ &\quad \left. - \frac{x^2}{q^2 c^2} [\alpha(ix) + \beta(ix)] [r_{\text{TM}}(ix, k_\perp) + r_{\text{TE}}(ix, k_\perp)] \right\}. \end{aligned} \quad (7)$$

Due to the presence of only one wall, the upper index on the reflection coefficients is omitted.

Using the so-called *proximity force approximation* (PFA), the Casimir force acting between a sphere and a plate can be expressed as

$$F(a, T) = 2\pi R \mathcal{F}(a, T), \quad (8)$$

where the free energy per unit area for two parallel semispaces is defined in Eq. (1). Under the condition that $a \ll R$, where R is the sphere radius and a is the closest separation between the surfaces of a sphere and a plate, the relative error of the approximate Eq. (8) is less than a/R [6, 8]. Equation (8) is widely used for the comparison of the experimental data obtained from the measurements of the Casimir force between a sphere and a plate with the predictions of the Lifshitz theory.

The original formulation of the Lifshitz theory for two parallel semispaces separated with a gap can be simply generalized for an arbitrary number of planar layers of different thickness made of arbitrary materials [23, 24, 25]. However, the obtaining of exact formulas for the Casimir free energy and force between bodies with nonplanar surfaces was challenging during the last few decades. The problem was solved in 2006 when several equivalent Lifshitz-type formulas were

obtained [26, 27, 28, 29] using the scattering theory and the formalism of functional determinants. Specifically, in one of the developed formalisms the Casimir free energy for two separated bodies of arbitrary shape labeled by the indices (1) and (2) can be presented in the form [30]

$$\mathcal{F}^{\text{exact}}(a, T) = k_B T \sum_{l=0}^{\infty} \ln \det \left[1 - \mathcal{T}^{(1)} \mathcal{G}_{\xi_l; (1,2)}^{(0)} \mathcal{T}^{(2)} \mathcal{G}_{\xi_l; (2,1)}^{(0)} \right]. \quad (9)$$

Here, $\mathcal{G}_{\xi_l; (1,2)}^{(0)}$ is the operator for the free space Green's function with the matrix elements $\langle \mathbf{r} | \mathcal{G}_{\xi_l; (1,2)}^{(0)} | \mathbf{r}' \rangle$, where \mathbf{r} belongs to the body (1) and \mathbf{r}' belongs to the body (2). $\mathcal{T}^{(1)}$ [$\mathcal{T}^{(2)}$] is the operator of T matrix for the body (1) [body (2)]. Using such representations, it was shown that for an ideal metal sphere above an ideal metal plate at room temperature the exact results for the Casimir force and for the thermal correction to it coincide with respective results obtained using the PFA in the zeroth order of the small parameter a/R [31].

Calculation of the Casimir force between real material bodies using the Lifshitz theory requires the availability of the respective $\varepsilon(\omega)$ and $\mu(\omega)$. We reserve the discussion of $\mu(\omega)$ for Sec. 4 and briefly consider here the dielectric permittivity for dielectrics and metals. It is common knowledge that all condensed bodies are either dielectrics or metals depending on the behavior of their dc conductivity $\sigma_0(T)$ when temperature vanishes [32, 33]. For dielectrics $\sigma_0(0) = 0$ whereas for metals $\sigma_0(0) \neq 0$. In this regard semiconductors are also either dielectrics or metals (specifically, intrinsic semiconductors are dielectrics, whereas doped semiconductors with dopant concentration above the critical value are metals). In the application of the Lifshitz theory to dielectric materials the small dc conductivity arising at $T \neq 0$ is usually neglected. In so doing the dielectric permittivities of dielectric plates are determined by the core electrons [34]

$$\varepsilon_c^{(n)}(\omega) = 1 + \sum_{j=1}^K \frac{g_j^{(n)}}{\omega_j^{(n)2} - \omega^2 - i\gamma_j^{(n)}\omega}, \quad (10)$$

where $\omega_j^{(n)} \neq 0$ are the oscillator frequencies, $g_j^{(n)}$ are the oscillator strengths, $\gamma_j^{(n)}$ are the damping parameters, and K is the number of oscillators. Note that the parameters of oscillators in Eq. (10) can be temperature-dependent. Thus, in addition to the explicit dependence on the temperature in Eqs. (1) and (6) through the multiple T and through the Matsubara frequencies, there is an implicit dependence through the dielectric permittivity. For Si such an implicit dependence was investigated in Ref. [35].

However, if one takes into account the existence of free charge carriers at $T \neq 0$, the dielectric permittivity of dielectric plates can be represented as [36]

$$\varepsilon_d^{(n)}(\omega) = \varepsilon_c^{(n)}(\omega) + i \frac{4\pi\sigma_0^{(n)}(T)}{\omega}. \quad (11)$$

It has been shown [37, 38] that the Casimir entropy calculated using the free energy (1) combined with the dielectric permittivity (10) satisfies an important thermodynamic constraint

$$S_c(a, T) = -\frac{\partial \mathcal{F}_c(a, T)}{\partial T} \rightarrow 0 \quad (12)$$

when $T \rightarrow 0$ (the Nernst heat theorem). If, however, the dc conductivity of dielectric material is taken into account [i.e., the dielectric permittivity (11) is used] we get [37, 38]

$$S_d(a, 0) = \frac{k_B}{16\pi a^2} \left[\zeta(3) - \text{Li}_3(r_0^{(1)} r_0^{(2)}) \right] > 0, \quad (13)$$

where

$$r_0^{(n)} = \frac{\varepsilon_c^{(n)}(0) - 1}{\varepsilon_c^{(n)}(0) + 1} < 1, \quad (14)$$

$\zeta(z)$ is the Riemann zeta function, and $\text{Li}_n(z)$ is the polylogarithm function. Keeping in mind that real dielectric materials possess dc conductivity, one arrives to the conclusion that for two parallel dielectric semispaces the Lifshitz theory violates the Nernst theorem.

A similar difficulty arises in the application of the Lifshitz theory to real metals. It is customary to describe the dielectric properties of metallic plates by means of the Drude model

$$\varepsilon_D^{(n)}(\omega) = 1 - \frac{\omega_p^{(n)2}}{\omega[\omega + i\gamma^{(n)}(T)]}, \quad (15)$$

where $\omega_p^{(n)}$ are the plasma frequencies and $\gamma^{(n)}(T)$ are the relaxation parameters. This model is well applicable in the wide frequency region from quasistatic frequencies (the normal skin effect) to infrared optics. It was shown [6, 8, 39, 40] that for perfect crystal lattices [where $\gamma^{(n)}(T) \rightarrow 0$ as T^2] the Casimir entropy calculated using the free energy (1) combined with the Drude model (15), violates the Nernst heat theorem

$$S_D(a, 0) = -\frac{k_B\zeta(3)}{16\pi a^2} \left[1 - \frac{2c}{a} \frac{\omega_p^{(1)} + \omega_p^{(2)}}{\omega_p^{(1)}\omega_p^{(2)}} + \frac{3c^2}{a^2} \left(\frac{\omega_p^{(1)} + \omega_p^{(2)}}{\omega_p^{(1)}\omega_p^{(2)}} \right)^2 - \dots \right] < 0. \quad (16)$$

Notice that for Drude metals with impurities there is a nonzero residual relaxation $\gamma_{\text{res}}^{(n)} = \gamma^{(n)}(0)$. In this case the Casimir entropy jumps abruptly to zero at $T < 10^{-4}$ K starting from a negative value (16), so that the Nernst theorem is formally satisfied [41, 42, 43]. This, however, does not solve the problem. The point is that a perfect crystal lattice is a truly equilibrium system with a nondegenerate dynamical state of the lowest energy. Thus, according to quantum statistical physics, the Casimir entropy calculated for a perfect crystal lattice must be equal to zero [44].

It is quite another matter when the nondissipative plasma model

$$\varepsilon_p^{(n)}(\omega) = 1 - \frac{\omega_p^{(n)2}}{\omega^2}, \quad (17)$$

is used instead of (15) to describe metallic plates. In this case the Nernst heat theorem is satisfied [6, 8, 39, 40], i.e.

$$S_p(a, T) = -\frac{\partial \mathcal{F}_p(a, T)}{\partial T} \rightarrow 0 \quad (18)$$

when $T \rightarrow 0$. It was proposed [6, 8, 45] that the inclusion of relaxation properties of free charge carriers in the model of dielectric response violates thermal equilibrium which is the basic applicability condition of the Lifshitz theory. This is because the drift electric current leads to a violation of time-reversal symmetry and requires the introduction of the unidirectional flux of heat from the Casimir plates to the heat reservoir to preserve the temperature constant. Consensus on the problem of why the Lifshitz theory is thermodynamically inconsistent in the presence of free charge carriers is not yet achieved.

To complete a brief survey of the Lifshitz theory, we mention recent attempts to modify the TM reflection coefficients by taking into account the effect of screening [46, 47]. This approach includes both the drift and diffusion currents of free charge carriers. Eventually the modified

TM reflection coefficient is obtained through the use of Boltzmann transport equation and takes the form [47]

$$r_{\text{TM}}^{(n)\text{mod}}(ix, k_{\perp}) = \frac{\varepsilon^{(n)}(ix)q - k^{(n)} - \frac{k_{\perp}^2}{\eta^{(n)}(ix)} \frac{\varepsilon^{(n)}(ix) - \varepsilon_c^{(n)}(ix)}{\varepsilon_c^{(n)}(ix)}}{\varepsilon^{(n)}(ix)q + k^{(n)} + \frac{k_{\perp}^2}{\eta^{(n)}(ix)} \frac{\varepsilon^{(n)}(ix) - \varepsilon_c^{(n)}(ix)}{\varepsilon_c^{(n)}(ix)}}. \quad (19)$$

Here, the dielectric permittivities of the plates are given by

$$\varepsilon^{(n)}(ix) = \varepsilon_c^{(n)}(ix) + \frac{\omega_p^{(n)2}}{x(x + \gamma^{(n)})}, \quad (20)$$

where permittivities of the bound core electrons $\varepsilon_c^{(n)}$ are defined in Eq. (10). The quantity $\eta^{(n)}(ix)$ is given by

$$\eta^{(n)}(ix) = \left[k_{\perp}^2 + \kappa^{(n)2} \frac{\varepsilon_c^{(n)}(0)}{\varepsilon_c^{(n)}(ix)} \frac{\varepsilon^{(n)}(ix)}{\varepsilon^{(n)}(ix) - \varepsilon_c^{(n)}(ix)} \right]^{1/2}, \quad (21)$$

where $1/\kappa^{(n)}$ are the screening lengths of plate materials [48] defined differently for dielectrics and metals (the Debye-Hückel and Tomas-Fermi screening lengths when the charge carriers are described by the Maxwell-Boltzmann and Fermi-Dirac statistics, respectively). The TE reflection coefficient in the proposed approach remains unchanged.

It was shown [45, 49, 50, 51], however, that the modification of the TM reflection coefficient in accordance with Eq. (19) also leads to the violation of the Nernst theorem for all dielectric materials whose charge carrier density does not vanish when $T \rightarrow 0$ and $\sigma_0(T)$ vanishes due to the vanishing mobility (for instance, for glasses with ionic conductivity [52] or doped semiconductors with dopant concentration below the critical value [53]). For metals with perfect crystal lattices the Lifshitz theory with the modified TM reflection coefficient violates the Nernst theorem in the same way as when the standard Drude model approach is used [50, 54, 55]. These conclusions were disputed in Refs. [56, 57], but the argumentation used was shown to be inadequate in Refs. [7, 50]. Therefore, the problem of consistency of the Lifshitz theory with thermodynamics for real materials remains unsolved.

3. Comparison with three landmark experiments

There are about 25 experiments on measuring the Casimir force in the modern stage of the work on the subject (see the review [6] for more details). In almost all experiments at least an attempt of comparing the measurement data with theory was undertaken. In this section, we consider only three experiments each of which, when carefully compared with the Lifshitz theory, leads to unexpected conclusions.

3.1. Measuring the Casimir pressure using a micromachined oscillator

The first of this landmark experiments was performed by R. S. Decca and his co-workers. It was repeated three times, in 2003 [9], 2005 [10], and in 2007 [11, 12] with major improvements in sample preparation and in the experimental precision in each repetition. The discussion below is related to the most precise experiment of 2007 [11, 12], where the gradient of the Casimir force between an Au-coated sphere of $R = 151.3 \mu\text{m}$ radius and a plate of micromachined oscillator was measured at $T = 300\text{K}$ in the dynamic regime (see Fig. 1 for the schematic diagram of a setup). In fact it was the shift of the resonant frequency of a micromachined oscillator that was

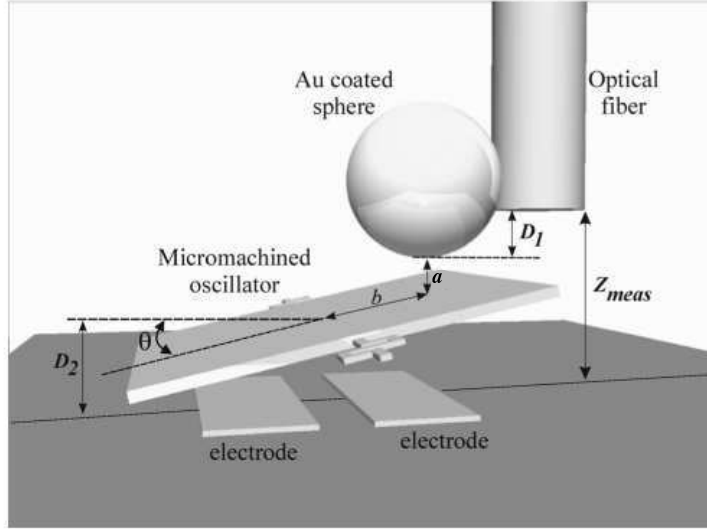


Figure 1. Schematic diagram of the setup for measuring the gradient of the Casimir force between a sphere and a plate (which is also an indirect measurement of the Casimir pressure between two parallel plates) using a micromachined oscillator.

measured. This shift is proportional to the gradient of the Casimir force between a sphere and a plate. Considering the negative derivative with respect to a of both sides of Eq. (8), one obtains

$$P(a, T) \equiv -\frac{\partial \mathcal{F}(a, T)}{\partial a} = -\frac{1}{2\pi R} \frac{\partial F(a, T)}{\partial a}. \quad (22)$$

Thus, the use of the PFA allows interpretation of the experiment by Decca et al. as an indirect measurement of the Casimir pressure between two parallel plates. In this experiment all errors were determined at a 95% confidence level, and the random errors were made much less than the systematic errors, so that only the latter determined the total experimental error. As a result, the total relative experimental error of the Casimir pressure varied from 0.19% at $a = 162$ nm to 0.9% at $a = 400$ nm and to 9.0% at the largest separation $a = 746$ nm. This includes the error of the PFA which was used to recalculate the experimental data for the gradient of the Casimir force into the Casimir pressure. In the most conservative way the error of the PFA was taken to be equal to a/R (specially performed experiment [58] and theoretical computations [59, 60, 61] for a sphere and a plate made of real metals described by the plasma and Drude models show that this error is in fact smaller than a/R).

Computations of the Casimir pressure between Au plates was performed by Eq. (1) with $\mu^{(n)} = 1$ using the tabulated optical data [36] for the complex index of refraction $n(\omega) = \text{Re} n(\omega) + i \text{Im} n(\omega)$. For this purpose the imaginary part of the dielectric permittivity of Au was found as $\text{Im} \varepsilon(\omega) = 2 \text{Re} n(\omega) \text{Im} n(\omega)$ at frequencies where the optical data are available and extrapolated to lower frequencies by means of the Drude model (15) with the parameters $\omega_p = 9.0$ eV, $\gamma = 0.035$ eV [62]. Then $\varepsilon(i\xi)$ for Au was obtained using the Kramers-Kronig relation

$$\varepsilon(i\xi) = 1 + \frac{2}{\pi} \int_0^\infty \frac{\omega \text{Im} \varepsilon(\omega)}{\xi^2 + \omega^2} d\omega. \quad (23)$$

This calculational approach corresponds to the use of the Drude model, as described in Sec. 2, but takes into account the role of core electrons. Keeping in mind that problems discussed in Sec. 2 originate from the zero-frequency term of the Lifshitz formula, one might expect that

related difficulties should appear here as well. For the comparison with the experimental data, the surface roughness on both the sphere and the plate was studied with the help of an atomic force microscope and taken into account in a nonmultiplicative way by means of geometrical averaging [6, 8].

Another approach to calculate the Casimir pressure between real metals with account of core electrons uses the generalized plasma-like model for the permittivity

$$\varepsilon(\omega) = \varepsilon_c(\omega) - \frac{\omega_p^2}{\omega^2}, \quad (24)$$

where $\varepsilon_c(\omega)$ is defined in Eq. (10) and the parameters of oscillators for Au with $K = 6$ were determined in Ref. [12]. The surface roughness is taken into account as described above.

Now we present a typical comparison between the experimental data and theory. In Fig. 2(a,b) the mean Casimir pressure together with the absolute experimental errors in the separation and pressure measured at different separations is shown as crosses. In Fig. 2(a) the theoretical Casimir pressure computed using the generalized plasma-like model and the optical data of Ref. [36] extrapolated by the Drude model is shown by the light-gray and dark-gray bands, respectively. The width of the bands indicates the total theoretical error. As can be seen in Fig. 2(a), the plasma-like model is consistent with the data, whereas a theory using the extrapolation to low frequencies by means of the Drude model is excluded by the data at a 95% confidence level. As was noted in the literature [63, 64], Au films prepared using different technology may possess different sets of optical data leading to the values of ω_p varying from 6.85 to 9.0 eV. In Fig. 2(b) the theoretical Casimir pressure as a function of separation computed with all sets of optical data available is shown as the dark-gray band. It is seen that the use of any alternative value of ω_p makes the disagreement between the Drude model approach and the data even more evident. One more recent experiment [65] incorporated the determination of the Casimir pressure by means of a micromachined oscillator with simultaneous measurement of the optical data of Au films. It was shown that while the Casimir pressures coincide with those measured previously in Refs. [11, 12], the optical data closely follow those tabulated in Ref. [36].

Another method for comparing theory with experiment considers the differences between theoretical and mean experimental Casimir pressures, $P^{\text{theor}}(a_i) - P^{\text{expt}}(a_i)$, and the 95%

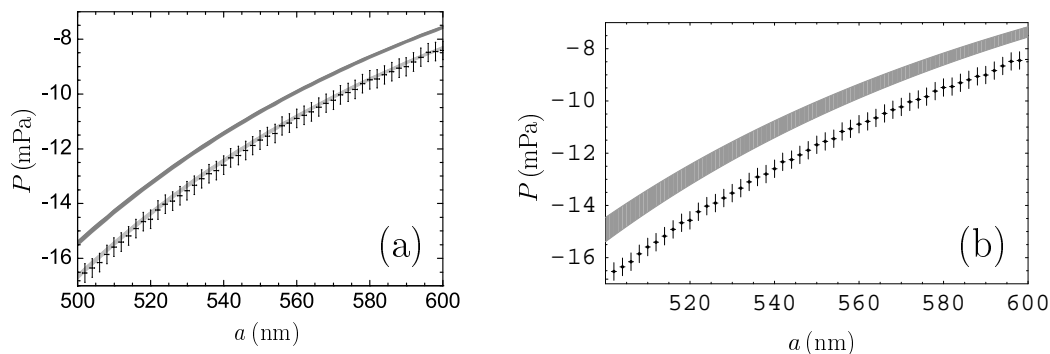


Figure 2. The measured mean Casimir pressure together with the absolute errors in the separation and pressure versus separation is shown as crosses. Errors are calculated at a 95% confidence level. (a) The theoretical Casimir pressure computed using the generalized plasma-like model and the optical data extrapolated by the Drude model is shown by the light-gray and dark-gray bands, respectively. (b) The theoretical Casimir pressure computed using different sets of optical data available in the literature versus separation is shown as the dark-gray band.

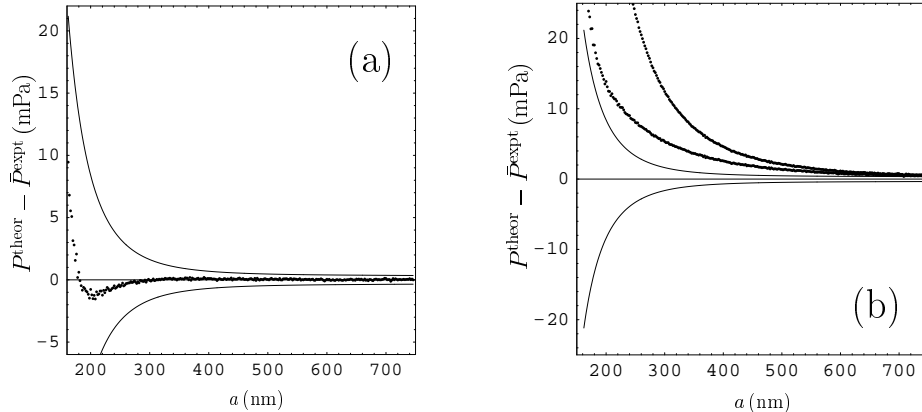


Figure 3. Differences between the theoretical Casimir pressures, computed by means of (a) the generalized plasma-like model and (b) the Drude model approach, and mean experimental Casimir pressures at different separations are shown as dots. The lower and upper sets of dots for the Drude model approach correspond to the use of maximum and minimum values of the plasma frequency available in the literature. The solid lines indicate the borders of the confidence intervals found at a 95% confidence level.

confidence interval $[-\Xi_P(a), \Xi_P(a)]$ to which 95% of these differences must belong if the theory is consistent with the data. In Fig. 3(a), the differences of the theoretically computed pressures using the generalized plasma-like model and mean experimental Casimir pressures are shown as dots. The solid lines are formed by the ends of the confidence intervals. As can be seen in Fig. 3(a), the Lifshitz theory using the generalized plasma-like model is consistent with the data. A similar comparison is made with the theoretical Casimir pressures computed using the tabulated optical data extrapolated by the Drude model. In Fig. 3(b) the differences $P^{\text{theor}}(a_i) - \bar{P}^{\text{expt}}(a_i)$ are indicated as two sets of dots computed using $\omega_p = 6.82 \text{ eV}$ (the upper set) and $\omega_p = 9.0 \text{ eV}$ (the lower set). The pressure differences for all other values of the plasma frequency of Au considered in Ref. [64] are between the two sets of dots in Fig. 3(b). Thus, theory using the Drude model is experimentally excluded over the entire measurement range from 162 to 746 nm at a 95% confidence level. Note that within a more narrow range of separations from 210 to 620 nm the theoretical approach using the Drude model is excluded by the data at a 99.9% confidence level [6, 8, 12]. The same data exclude [66] the Lifshitz theory at zero temperature combined with the Drude model. This exclusion is made at a 70% confidence level with the optical data of Ref. [36] and at 95% confidence level with the alternative optical data.

The experimental data of Ref. [11, 12] have been also compared with theoretical predictions obtained using the modified TM reflection coefficient (19). In so doing it was supposed that electrons in Au are described by Fermi-Dirac statistics. Almost the same computational results for the Casimir pressure were obtained [50, 54, 55], as by using the Drude model. Thus, the Lifshitz theory with the modified TM reflection coefficient is excluded by the experiment of Refs. [11, 12].

3.2. Optical modulation of the Casimir force

The second landmark experiment was performed by U. Mohideen and his co-workers [13, 14]. In this experiment, an atomic force microscope was employed to measure the change in the Casimir force between an Au-coated sphere ($R = 98.9 \mu\text{m}$) and a Si membrane at $T = 300 \text{ K}$ in the presence and in the absence of incident laser light on a membrane (see schematic of the experimental setup in Fig. 4). The experiment was repeated three times with three different

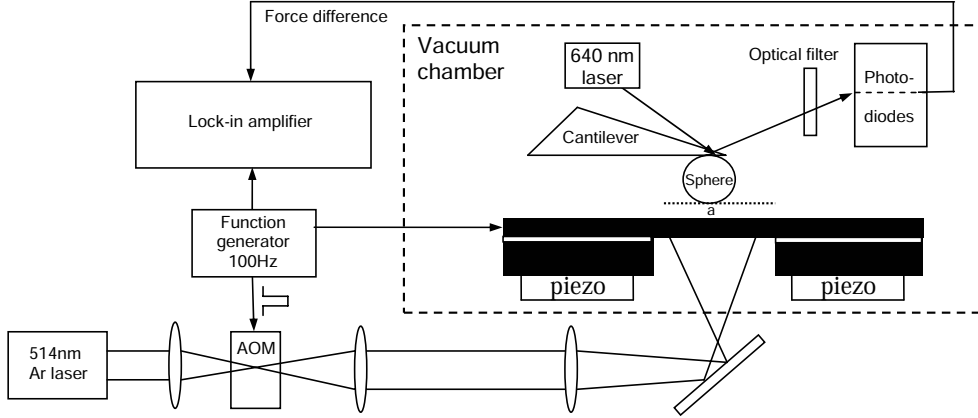


Figure 4. Schematic of the experimental setup on measuring the difference Casimir force between Au sphere and Si plate illuminated with laser pulses.

absorbed laser powers. The values of the maximum and minimum absorbed powers were equal to $P_a = 9.3 \text{ mW}$ and $P_b = 4.7 \text{ mW}$. In the absence of laser light, the charge carrier density of high-resistivity Si was $n_h = 5 \times 10^{14} \text{ cm}^{-3}$. In the presence of light, the charge carrier densities related to the maximum and minimum absorbed powers took the values $n_a = (2.1 \pm 0.4) \times 10^{19} \text{ cm}^{-3}$ and $n_b = (1.4 \pm 0.3) \times 10^{19} \text{ cm}^{-3}$ (the errors are indicated at a 95% confidence level [14]).

The difference of the theoretical Casimir forces in the presence and in the absence of laser light,

$$F_{\text{diff}}^{\text{theor}}(a, T) = F_l^{\text{theor}}(a, T) - F^{\text{theor}}(a, T), \quad (25)$$

was calculated using Eq. (1) with $\mu^{(n)} = 1$ and Eq. (8), taking into account the surface roughness by means of geometrical averaging. The dielectric permittivity of the Au-coated sphere $\varepsilon^{(1)}(i\xi) \equiv \varepsilon_{\text{Au}}(i\xi)$ is described by Eq. (24). The dielectric permittivity of the Si plate $\varepsilon^{(2)}(i\xi) \equiv \varepsilon_{\text{Si}}(i\xi)$ depends on the concentration of charge carriers. In the absence of charge carriers (infinitely high resistivity) it was computed by using the tabulated optical data [36] and the Kramers-Kronig relation. The obtained results, $\varepsilon_{\text{Si},0}(i\xi)$, are shown by the dashed line in Fig. 5(a). The dielectric permittivity of high-resistivity plate used in the experiment in the absence of laser light, $\varepsilon_{\text{Si},h}(i\xi)$, can be presented as the sum of $\varepsilon_{\text{Si},0}(i\xi)$ and the second term on the right-hand side of Eq. (11) taking the dc conductivity into account. In Fig. 5(a) the quantity $\varepsilon_{\text{Si},h}(i\xi)$ is shown by the dotted line. Similarly, the dielectric permittivity of low-resistivity Si with different absorbed powers, $\varepsilon_{\text{Si},a,b}(i\xi)$, are shown by the solid lines a and b taking into account both electrons and holes [67, 68, 69].

Now we are in a position to compare the experimental data with the predictions of the Lifshitz theory. In Fig. 5(b) the mean experimental differences, $\bar{F}_{\text{diff}}^{\text{expt}}$, of the Casimir forces in the presence and in the absence of laser light for the absorbed power P_b are shown as crosses. The arms of the crosses represent total experimental errors in the measurement of the difference force and separation distance, determined at a 95% confidence level. The theoretical differences of the Casimir force (25) were first computed using the dielectric permittivity $\varepsilon_{\text{Si},h}(i\xi)$ in the absence of light which takes the dc conductivity of a Si plate into account. In the presence of light the permittivity $\varepsilon_{\text{Si},b}(i\xi)$ has been used. The computational results are presented by the dashed line in Fig. 5(b). As can be seen in the figure, the prediction of the Lifshitz theory taking into account the dc conductivity of high-resistivity Si is experimentally excluded. Then the theoretical differences (25) were computed using the dielectric permittivity $\varepsilon_{\text{Si},0}(i\xi)$ in the

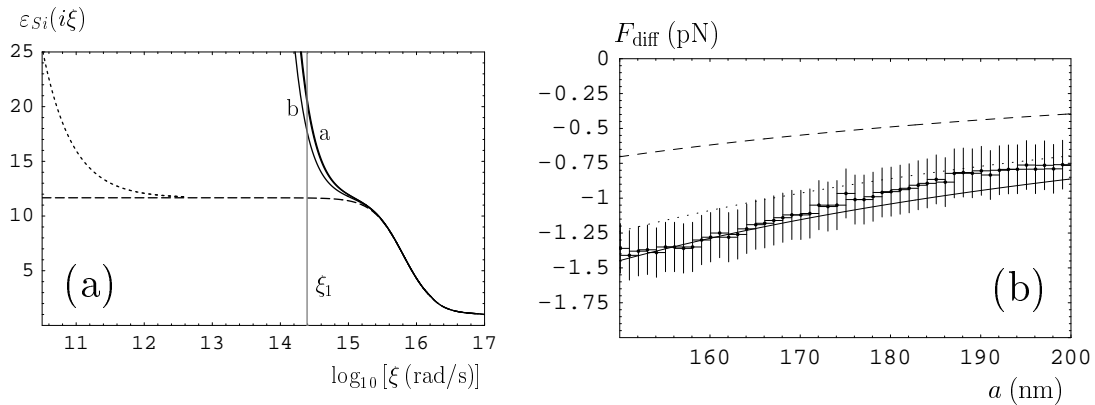


Figure 5. (a) The dielectric permittivity of the Si membrane along the imaginary frequency axis for Si with different concentration of charge carriers (see text for further discussion). The vertical gray line indicates the first Matsubara frequency at $T = 300$ K. (b) The experimental differences in the Casimir force with their experimental errors are shown as crosses (the absorbed power is equal to 4.7 mW). The solid and dotted lines represent the theoretical differences computed at $T = 300$ K using the model with a finite static permittivity of high-resistivity Si, but different models for Si in the presence of light (see text for further discussion). The dashed line represents the theoretical differences computed including the dc conductivity of high-resistivity Si.

dark phase which disregards the dc conductivity of Si. In the presence of light the permittivity $\varepsilon_{Si,b}(i\xi)$ was again used. In this case the computational results are shown by the solid line in Fig. 5(b) which is consistent with the data.

Note that the dielectric permittivity $\varepsilon_{Si,b}(i\xi)$ used in the presence of light describes charge carriers in the low-resistivity Si by means of the Drude model. If to take into account that n_b is larger than the critical value of charge carrier density indicating the dielectric to metal phase transition, it would be reasonable to use the description by means of the generalized plasma-like model in the presence of light (see Sec. 2). The computational results obtained within this approach [70] are presented by the dotted line in Fig. 5(b). It is seen that the dotted line is consistent with the data, as well as the solid line. Thus, this experiment is not of sufficient precision to discriminate between the description of charge carriers in metallic phase by means of the Drude and plasma models (this was done by the experiment of Decca et al. considered in Sec. 3.1). The main new and unexpected result of the experiment by Mohideen et al. is that the inclusion of the dc conductivity in a dielectric phase (high-resistivity Si) results in the contradiction of the Lifshitz theory with the data. Because of this, phenomenologically one may conclude [38] that in applications of the Lifshitz theory to dielectric materials the dc conductivity should be disregarded. Note that the contribution of dc conductivity to the dielectric permittivity of dielectrics was also disregarded when studying nonequilibrium thermal fluctuations of the electric field in the presence of a dc current [71].

The experimental data of the optical modulation experiment was compared with the modified Lifshitz theory using the TM reflection coefficient (19) proposed in Refs. [46, 47]. It was found that predictions of the modified Lifshitz theory for the Si plate in a dielectric phase cannot be excluded at a 95% confidence level. Because of this, the comparison has been made at a 70% confidence level [45]. In Fig. 6(a) the experimental data for the measured difference Casimir force in the presence and in the absence of light are shown as crosses. When compared to Fig. 5(b), the arms of the crosses are made relatively shorter, as required by a lower confidence level. The prediction of the modified Lifshitz theory for the absorbed power P_b is shown as a band bounded by the two dashed lines. The width of this band is found from the theoretical error determined mostly by the error in n_b (at a 70% confidence level this error is equal to

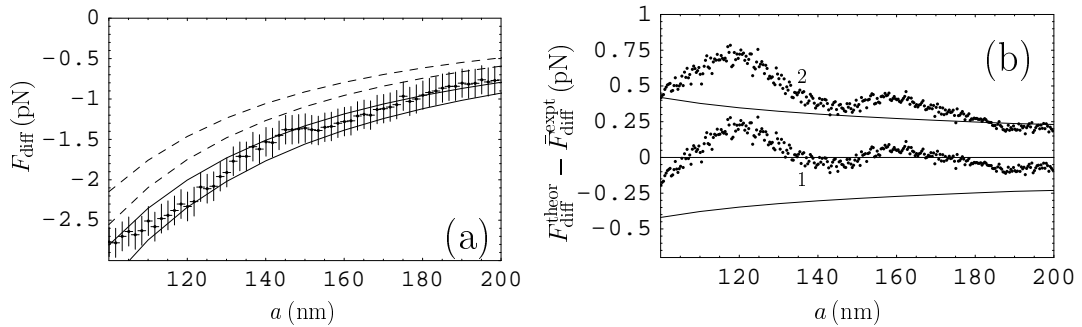


Figure 6. (a) The measured force differences are shown as crosses versus separation a . The two theoretical bands lie between the solid and dashed lines (see text for details). (b) Theoretical minus mean experimental differences of the Casimir force versus separation are shown as dots. For the dots labeled 1, the theoretical results are computed with a finite static dielectric permittivity of high resistivity Si in the absence of laser pulse and using the plasma model to describe the charge carriers when the laser pulse is on. For dots labeled 2, the theoretical results are computed in the framework of the modified Lifshitz theory [46, 47]. The solid lines indicate 70% confidence intervals including all experimental and theoretical errors.

$0.22 \times 10^{19} \text{ cm}^{-3}$ to compare with $0.3 \times 10^{19} \text{ cm}^{-3}$ at a 95% confidence level). The prediction of the standard Lifshitz theory with dc conductivity of Si in the absence of light disregarded is shown by the band bounded by two solid lines. The width of this band also corresponds to an error in n_b determined at a 70% confidence level. As can be seen in Fig. 6(a), the predictions of the modified Lifshitz theory [46, 47] are excluded by the data at a 70% confidence level, whereas the standard Lifshitz theory with disregarded dc conductivity of dielectric Si is consistent with the data.

The same conclusion can be obtained when using another approach to the comparison between experiment and theory similar to that in Fig. 3. In Fig. 6(b) the differences between theoretical and mean experimental difference Casimir forces, $F_{\text{diff}}^{\text{theor}} - \bar{F}_{\text{diff}}^{\text{expt}}$, at different separations are plotted as the two sets of dots. The set labeled 1 is computed using the standard Lifshitz theory with the dc conductivity of dielectric Si disregarded. The set labeled 2 is computed using the modified Lifshitz theory. The two solid lines indicate the borders of a 70% confidence intervals determined with account of all experimental and theoretical errors. It is seen that the standard Lifshitz theory with the dc conductivity disregarded is consistent with the data, whereas the modified Lifshitz theory [46, 47] is excluded by the measurement results of the optical modulation experiment at a 70% confidence level.

3.3. Measurements of the thermal Casimir-Polder force

The third landmark experiment is on measuring the Casimir-Polder force between ground state ^{87}Rb atoms and a fused silica plate. It was performed by Cornell and his co-workers [15]. Atoms of ^{87}Rb belonged to the Bose-Einstein condensate separated by a distance of a few micrometers from a wall. The experiment was of dynamic-type. The dipole oscillations in the direction perpendicular to the plate with the frequency ω_0 were excited in a condensate, and the relative shift of this frequency

$$\gamma_z = \frac{|\omega_0 - \omega_z|}{\omega_0} \quad (26)$$

due to the Casimir-Polder interaction was measured precisely. This shift can be recalculated [72] into the Casimir-Polder force (6) with $\mu^{(n)} = 1$, $\beta(i\xi) = 0$ leading to its indirect measurement.

This experiment was repeated three times, once in thermal equilibrium, when the temperature of the plate was equal to the environment temperature, $T_p = T_e = 310$ K, and two times with $T_p > T_e$ (in the latter case there are additions to the Casimir-Polder force (6) calculated in Ref. [73]). The relative frequency shift (26) was measured at several atom-plate separations in the region from 7 to 11 μm . Keeping in mind that the comparison of the frequency shift with the Casimir-Polder force includes an averaging over the condensate cloud, the role of atom-plate separation is in fact played by the distance between the plate and the center of mass of the condensate.

In Fig. 7(a) the experimental data for the relative frequency shift γ_z in thermal equilibrium at separations below 10 μm are shown as crosses [15]. The arms of the crosses indicate total experimental errors in the measurement of γ_z and separation distances at a 66% confidence level found at each experimental point separately using the analysis of Ref. [74]. To compare the experimental data with theory, in Ref. [15] the relative frequency shift (26) was computed using the Lifshitz formula (6) for the Casimir-Polder force and an averaging over the condensate cloud. In so doing the static value for the polarizability of Rb atom $\alpha(0) = 4.73 \times 10^{-23}$ cm^3 can be used. The dielectric permittivity of fused silica $\varepsilon(i\xi_l)$, as a function of ξ_l , can be calculated [75] using the tabulated optical data [36] and the Kramers-Kronig relation (19). In the original Ref. [15] it was assumed that the fused silica is a true dielectric of infinitely high resistivity. Thus, the dc conductivity of the plate was disregarded. Under this assumption the obtained theoretical results [15] are shown by the solid line in Fig. 7(a). It is seen that the Lifshitz theory of the Casimir-Polder interaction with the dc conductivity of fused silica disregarded is consistent with the measurement data.

It should be noted, however, that although fused silica is a good insulator, it possesses a nonzero conductivity at $T_p = 310$ K. This conductivity is ionic in nature and is determined by the concentration of impurities (alkali ions). In Ref. [16] the computations of Ref. [15] were repeated both disregarding and including the dc conductivity of fused silica. When the dc conductivity was disregarded, the results of Ref. [15] given by the solid line were reproduced. When, however, the dc conductivity was included, quite different results were obtained shown by the dashed line in Fig. 7(a). It is seen that with inclusion of the dc conductivity the Lifshitz theory is inconsistent with at least two experimental points at shortest separations.

The second and third repetitions of the experiment of Ref. [15] were performed with the

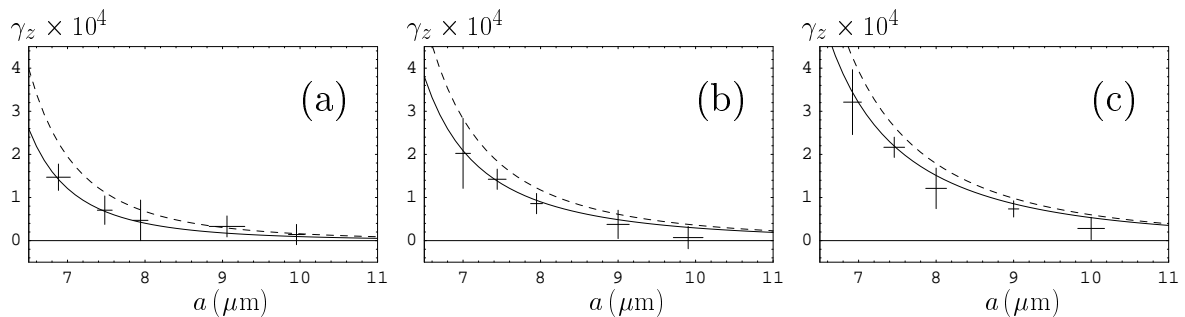


Figure 7. The fractional change in the trap frequency versus separation (a) in thermal equilibrium with $T_p = T_e = 310$ K and out of thermal equilibrium (b) with $T_p = 479$ K and $T_e = 310$ K and (c) with $T_p = 605$ K and $T_e = 310$ K. Computations are done by neglecting (solid lines) and including (dashed lines) the dc conductivity of the dielectric plate. The experimental data are shown as crosses.

same temperature of environment, $T_e = 310$ K, but with increased temperatures of the plate, $T_p = 479$ K and 605 K, respectively. The obtained experimental data are shown as crosses in Fig. 7(b) for $T_p = 479$ K and Fig. 7(c) for $T_p = 605$ K. The computational results of Ref. [15] disregarding the dc conductivity of fused silica are shown as the solid lines in Fig. 7(b,c). They were reproduced in Ref. [16] under an assumption that the dc conductivity of fused silica is omitted. As is seen in Fig. 7(b,c), the solid lines are in a good agreement with the experimental data. In Ref. [16] computations of the relative frequency shift γ_z for the second and third repetitions of the experiment with increased temperature of the plate were performed taking the dc conductivity of fused silica into account. The computational results shown by the dashed lines in Fig. 7(b,c) differ dramatically from the results obtained with the dc conductivity disregarded. As can be seen in Fig. 7(b), the three experimental points for $T_p = 479$ K exclude the dashed line and the other two only touch it. As to the dashed line in Fig. 7(c), it is seen that all data points at $T_p = 605$ K exclude the theoretical prediction computed taking the dc conductivity of fused silica into account. Thus, measurements of the thermal Casimir force between ^{87}Rb atoms and fused silica plate suggest that in the application of the Lifshitz theory to dielectric materials the dc conductivity of these materials should be omitted.

In fact, the results of all three landmark experiments performed by three different experimental groups are in agreement. According to these results, the relaxation properties of free charge carriers are irrelevant to the phenomenon of dispersion forces and should be disregarded. For metals characterized by a high density of charge carriers, they should be accounted for by means of the plasma model. For dielectrics charge carriers should be ignored. If this phenomenological prescription [6, 8, 38, 70] is used, the Lifshitz theory agrees well with all available experimental data.

4. Possibilities to control the magnitude and sign of the Casimir force

Applications of the Casimir force to nanotechnology require some operational means to modify the force magnitude at a fixed separation distance and even change the force sign with varying separation. This would permit to realize the actuation of devices with the Casimir force at a nanoscale and, when necessary, avoid such undesired effects as pull-in and stiction mentioned in Sec. 1. Below we briefly discuss different possibilities to control the Casimir force proposed in the literature some of which were already tested experimentally. Special attention is paid to magnetic materials which could significantly widen the role of Casimir forces in applied science. Here, we do not discuss the Casimir force between metamaterials because the application of the Lifshitz formula to such materials is questionable, and corresponding experimental data are not yet available. In spite of repeated speculations on the possibility of Casimir repulsion, it was shown [76] that the Casimir force between two plates made of metamaterials and separated by a vacuum gap is always attractive.

4.1. Different ways of modifying dielectric properties

To modify the magnitude of the Casimir force, the dielectric properties of interacting bodies should be changed over a wide frequency region. The most apparent possibility of decreasing the magnitude of the Casimir force, as compared with the case of two metallic test bodies, is to make one of them of a semiconductor or dielectric (or at least to cover them with sufficiently thick dielectric coating). As an example, in the experiment of Refs. [77, 78] the Casimir force acting between a Au coated sphere and Si plate at $a = 100$ nm in vacuum was of about 30% less than between the same Au sphere and a Au plate. In the experiment of Ref. [79] the Casimir forces acting between a Au sphere and two Si plates with significantly different dopant concentrations were sequentially measured. The density of charge carriers in the first plate was $n_a \approx 1.2 \times 10^{16} \text{ cm}^{-3}$ and in the second plate $n_b \approx 3.2 \times 10^{20} \text{ cm}^{-3}$. It was found that by choosing plates with such different concentrations of charge carriers the Casimir force acting

between a Au sphere and a Si plate can vary by 5% and 8% at separations $a = 60$ and 100 nm, respectively. In Ref. [80] the measured values of the Casimir force between Au sphere and Au plate were compared with respective measurements resulted from a Au sphere and a glass plate covered with a 190 nm layer of indium tin oxide which is a conductor at low frequencies (with respect to the Casimir force this material was first discussed in Ref. [39]). Within the separation region from 50 to 150 nm the Casimir force between a sphere and a plate covered with indium tin oxide was shown to be 40%–50% less than between the same sphere and a Au plate.

The use of test bodies made of dielectric material or coated with dielectric layers allows to decrease the magnitude of the Casimir force but does not allow to change this magnitude periodically. The latter was realized in the optical modulation experiment of Refs. [13, 14] considered in Sec. 3.2. In this experiment, the differences of the Casimir forces in the presence and in the absence of laser light on a Si plate are equal to 3% and 6.5% of the Casimir force in the absence of light at separations $a = 100$ and 150 nm, respectively. It is important that here the magnitude of the Casimir force varies periodically as long as the laser operated in the pulse mode is switched on.

Optical modulation of the Casimir force in vacuum makes it possible to periodically change the magnitude of the Casimir force but does not allow to replace attraction with repulsion. Considerable opportunities for nanotechnology would be opened up if pulsating Casimir plates were possible, moving back and forth under the action of the Casimir force without use of micromechanical springs. This can be achieved only by using both attractive and repulsive Casimir forces. In this respect, it should be noted that there is the case where the Casimir repulsion is well understood, i.e., the repulsion between the two plates described by the dielectric permittivities $\varepsilon^{(1,2)}(i\xi)$ separated with a liquid layer having the dielectric permittivity $\varepsilon^{(0)}(i\xi)$ such that [5, 6, 8]

$$\varepsilon^{(1)}(i\xi) < \varepsilon^{(0)}(i\xi) < \varepsilon^{(2)}(i\xi). \quad (27)$$

The Casimir repulsion in three-layer systems was observed in Refs. [81, 82, 83, 84] (see also Refs. [85, 86] concerning additional difficulties arising for measurements of the Casimir force in liquids).

Recently it was shown [87] that the illumination of one (Si) plate in three-layer systems Au–ethanol–Si, Si–ethanol–Si, and α -Al₂O₃–ethanol–Si with laser pulses can change the Casimir attraction to the Casimir repulsion and vice versa. This allows to combine the advantages of the optical modulation with the Casimir repulsion in three-layer systems. As a result, one can obtain attraction and repulsion interchangeably at regular intervals. Calculations show [87] that in the system Au–ethanol–Si the Casimir force is repulsive at $a > 160$ nm. The illumination of the Si plate with laser light changes this repulsion for attraction. In the system Si–ethanol–Si, the Casimir force between the Si plates is attractive in the absence of laser light. However, when one of the two Si plates is illuminated, the attraction is replaced with repulsion at separations $a > 175$ nm [87]. In both these systems the magnitude of the repulsive pressure is several times less than the magnitude of the attractive pressure at the same separation. However, in the three-layer system α -Al₂O₃–ethanol–Si, where the Si plate is illuminated with laser pulses, the light-induced Casimir repulsion is of the same order of magnitude as the Casimir attraction. Specifically, in this system in the presence of light the Casimir repulsion arises at $a > 70$ nm. Thus, at $a = 110$ nm the attractive Casimir pressure in the absence of light is equal to about -75 mPa, whereas the repulsive pressure in the presence of light is equal to 50 mPa.

The dielectric properties undergo changes during different phase transitions. It was shown [88] that the change in the Casimir free energy associated with the phase transition of a metal to the superconducting state is very small. Nevertheless, according to Refs. [89, 90], the magnitude of this change is comparable to the condensation energy of a superconducting film and causes a measurable increase in the value of the critical magnetic field. It was also proposed [91] to measure the change of the Casimir force in a superconducting cavity due to a small change of

temperature.

Considerable change of the dielectric properties occurs in semiconductor materials that undergo a dielectric-metal phase transition with an increase in temperature. It was proposed [92] to measure the change of the Casimir force acting between an Au-coated sphere and a vanadium dioxide (VO₂) film deposited on a sapphire substrate, where the VO₂ undergoes a phase transition. At $T = 68^\circ\text{C}$ thin VO₂ films undergo an abrupt transition from a dielectric-type semiconductor to a metallic phase. During this phase transition the resistivity of the film decreases by a factor 10^4 from 10 to $10^{-3}\ \Omega\ \text{cm}$. The increase in temperature necessary for the phase transition can be induced by laser light. Thus, a setup similar to the one described in Sec. 3.2 can be used. Preliminary theoretical results using the optical data for VO₂ films show [92, 93] that the difference Casimir force between a Au sphere and VO₂ film after and before the phase transition is sensitive to the model of conductivity properties used in computations. Thus, this experiment may help in the resolution of the problems discussed in Secs. 2 and 3.

Another type of dielectric-metal phase transitions leading to the change of dielectric properties is a transition from amorphous to crystalline state in AgInSbTe. In Ref. [94] the gradient of the Casimir force between a Au coated sphere of $20.2\ \mu\text{m}$ diameter and $1\ \mu\text{m}$ thick AgInSbTe films deposited onto Al-coated Si substrates was measured using an atomic force microscope in dynamic mode. Half of the films were amorphous and the other half were annealed to the metallic crystalline phase. It was shown that differences in the gradient of the Casimir force between a sphere and an amorphous film on the one hand and between a sphere and a crystalline film on the other hand achieve 20% at separations of about 100 nm. The obtained experimental results were compared with computations using the Lifshitz theory and significant deviations were found. Taking into account that according to Ref. [94] the role of surface roughness was negligible at separations above 70 nm, these deviations might be explained by the influence of localized charges in the amorphous phase and by the use of the Drude model in the extrapolation of the optical data in the crystalline phase where AgInSbTe exhibits metallic conductivity (see Secs. 2 and 3).

4.2. Prospects of using magnetic materials

The possibility to modify the magnitude of the Casimir force and even to change attraction for repulsion has long been discussed in the literature. Specifically, in Ref. [95] the Casimir pressure between two magnetodielectric plates was investigated in the approximation of frequency-independent ε and μ . For sufficiently large μ repulsive forces were found. It was commented in the literature, however, that for real magnetic materials μ is nearly equal to unity in the range of frequencies, which gives major contribution to the Casimir force [96]. As a result, the magnitude of μ always remains far away from the values needed to get the Casimir repulsion. In fact the largest magnitude of $\mu(i\xi)$ is achieved at $\xi = 0$. For diamagnets [97] $|\mu(0) - 1| \sim 10^{-5}$ always. Thus, these materials cannot be used for modifying the magnitude of the Casimir force. For paramagnets, with the single exception of ferromagnets, the deviation of $\mu(0)$ from unity is also negligibly small at any temperature [97].

The subset of paramagnetic materials called *ferromagnets* requires special attention when the aim is to modify the Casimir force. For such materials $\mu(0) \gg 1$ at temperatures lower than the so-called *Curie* temperature T_c [97]. The values of $\mu(i\xi)$ for ferromagnets, however, quickly decrease with the increase of frequency. Thus, for ferromagnetic metals $\mu(i\xi)$ drops toward unity at frequencies of order 10^5 Hz and for ferromagnetic dielectrics at frequencies of order 10^9 Hz (note that the first Matsubara frequency ξ_1 at $T = 300$ K is of order 10^{14} Hz). Because of this, in all computations using Eq. (1) at, say, $T > 0.3$ K one can put $\mu(i\xi_l) = 1$ at all $l \geq 1$ and include ferromagnetic properties only in the zero-frequency term with $l = 0$ [98, 99].

Recently the formalism of functional determinants discussed in Sec. 2 was applied to calculate the Casimir force acting between an ideal metal cylinder far away from a magnetodielectric

plate [100]. Calculations were performed at $T = 0$. It was argued that for a cylinder remote sufficiently far from the plate, it is justified to use the static values $\varepsilon(0)$ and $\mu(0)$ for the dielectric permittivity and static permeability of the plate material. Under these assumptions, both attractive and repulsive Casimir force was obtained depending on the values of $\varepsilon(0)$ and $\mu(0)$. It should be remarked, however, that in order for magnetic properties to influence the Casimir force, the characteristic frequency $\omega_c = c/(2a)$ must be less than 10^9 Hz. Hence it follows that cylinder-plate separation must be larger than 15 cm. At such large separations any discussion concerning the sign of the Casimir force seems problematic, because this force is equal to zero for all practical purposes and is considerably dominated by Newtonian gravity. As was shown in Ref. [101], the calculational results for the Casimir force between magnetodielectric materials with frequency-dependent μ depend crucially on whether the zero-temperature or thermal Lifshitz formula is used.

The investigation of thermal Casimir interaction between two magnetodielectric plates with account of real material properties was performed in Refs. [98, 99]. As is clear from the foregoing, only ferromagnets may show noticeable effect on the Casimir force. With respect to the Casimir effect, however, it is not reasonable to consider parallel plates made of so-called *hard* ferromagnetic materials which possess spontaneous magnetization. The point is that the magnetic interaction between such plates far exceeds any conceivable Casimir force. Ferromagnetic materials discussed below are what is referred to as *soft* ferromagnetic materials, which do not possess spontaneous magnetization. It is well known also [97] that the magnetic permeability of ferromagnets depends on the applied magnetic field (the so-called *hysteresis*). Keeping in mind that no external magnetic field is applied to the Casimir plates and that the mean value of the fluctuating magnetic field is equal to zero, one should consider what is often referred to as *initial* permeability, i.e., $\mu(\mathbf{H} = 0)$.

Now we present a few computational results illustrating the impact of ferromagnetic materials on the magnitude and sign of the Casimir force. Computations of the Casimir pressure were performed using Eq. (1) at room temperature with ferromagnetic properties included in the zero-frequency term $l = 0$. The dielectric properties of ferromagnetic and nonmagnetic metallic plates are described either by the Drude model (15) or by the plasma model (17) and the obtained results are compared. Keeping in mind that ferromagnetic properties contribute only through the zero-frequency term, it is reasonable to consider not too short separations where the relative contribution of this term is more pronounced. Below we consider separation distances from 0.5 to $6 \mu\text{m}$, where the role of core electrons in the dielectric response can be neglected.

First we consider the Casimir pressure between two plates made of the ferromagnetic metal Co with $\mu_{\text{Co}}^{(n)}(0) = 70$ [102]. The Drude parameters of Co are the following [103]: $\omega_{p,\text{Co}}^{(n)} = 3.97$ eV and $\gamma_{\text{Co}}^{(n)} = 0.036$ eV. The computational results are presented as a ratio to the zero-temperature Casimir pressure between two nonmagnetic plates made of ideal metal at zero temperature

$$P_0(a) = -\frac{\pi^2 \hbar c}{240 a^4}. \quad (28)$$

In Fig. 8, the solid and dashed lines show the values of P_{Co}/P_0 as functions of separation computed using the dielectric permittivity (a) of the Drude model and (b) of the plasma model with account of magnetic properties and with magnetic properties disregarded, respectively. Quantitatively, the role of magnetic properties can be characterized by the ratio

$$\eta_{P,\text{Co}}(a, T) = \frac{P_{\text{Co}}^{\text{solid}}(a, T) - P_{\text{Co}}^{\text{dashed}}(a, T)}{P_{\text{Co}}^{\text{dashed}}(a, T)}. \quad (29)$$

With the increase in separation from 0.5 to $2 \mu\text{m}$ and then to $6 \mu\text{m}$, $\eta_{P,\text{Co}}^D$ computed using the Drude model varies from 12% to 44% and to 92%, respectively. Thus, when the Drude model

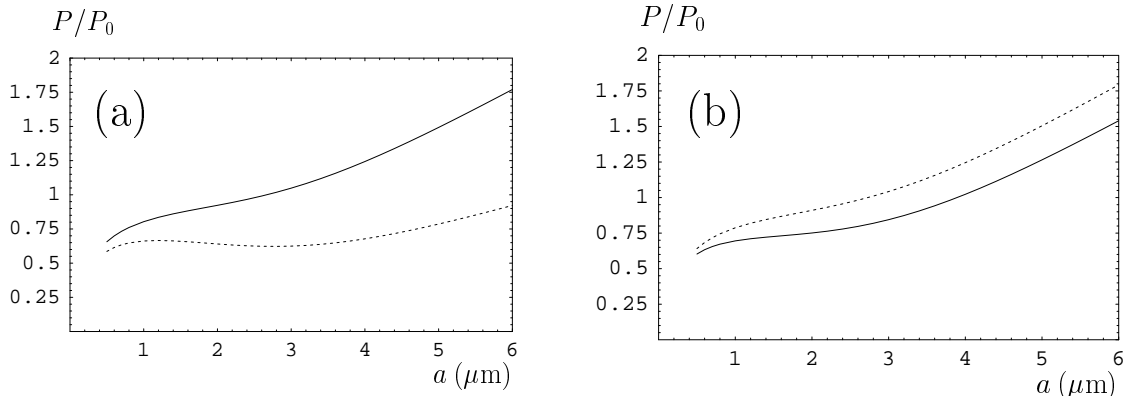


Figure 8. The relative Casimir pressures as functions of separation in the configuration of two parallel Co plates with account of magnetic properties (solid lines) and with magnetic properties disregarded (dashed lines). Computations are performed at $T = 300$ K using (a) the Drude model and (b) the plasma model for the dielectric permittivity.

is used to describe the dielectric properties of a ferromagnetic metal, the magnetic properties markedly (up to almost two times at large separations) increase the magnitude of the Casimir pressure [98]. As can be seen in Fig. 8(b), for ferromagnetic metal described by the plasma model the impact of magnetic properties on the Casimir pressure is not so pronounced. Quantitatively, from Fig. 8(b) it follows that at separation 0.5 , 2 , and $6 \mu\text{m}$ $\eta_{P,\text{Co}}^p$ varies from -6% to -17% , and to -14% , respectively. Mention should be made that if the plasma model is used, the inclusion of magnetic properties decreases the magnitude of the Casimir pressure. Similar results were also obtained for Fe [98]. In both cases the inclusion of the magnetic properties does not change the sign of the Casimir force leaving it attractive.

Very prospective materials for the investigation of the impact of magnetic properties on the Casimir force are ferromagnetic dielectrics. These materials, while displaying physical properties characteristic for dielectrics, demonstrate ferromagnetic behavior under the influence of an external magnetic field [104]. Many ferromagnetic dielectrics are, for instance, composite materials obtained on the basis of a matrix of a polymer compound with inclusion of nanoparticles of ferromagnetic metals. As was shown in Ref. [98], the Casimir force between two parallel plates made of ferromagnetic dielectric remains attractive, while the influence of magnetic properties on the Casimir pressure is much stronger than for Co plates considered above.

Here, we consider the configuration of one plate made of ferromagnetic dielectric ($n = 1$) and the other plate made of a nonmagnetic metal Au ($n = 2$). As is shown below, in this configuration the results for the Casimir pressure are drastically different depending on whether the Drude or the plasma model is used for the description of Au. In the case when the Drude model is used, from Eqs. (4) and (15) it follows that $r_{\text{TE}}^{(2)}(0, k_{\perp}) = 0$. Keeping in mind that at zero frequency magnetic properties do not influence the TM reflection coefficient, we arrive at the conclusion that if the Drude model is used for the description of Au there is no impact of magnetic properties on the Casimir pressure between gold and magnetodielectric plates. To perform computations when Au plate is described by the plasma model, one should choose some specific ferromagnetic dielectric. We consider the composite material on the basis of polystyrene with the volume fraction of ferromagnetic particles in the mixture $f = 0.25$. The magnetic permeability of such materials may vary over a wide range [105]. Below we use $\mu(0) = 25$. The dielectric permittivity of polystyrene $\varepsilon_d(i\xi)$ is presented in the form (10) with $K = 4$. The parameters of oscillators can be found in Ref. [34] leading to $\varepsilon_d(0) = 2.56$. As a result, the

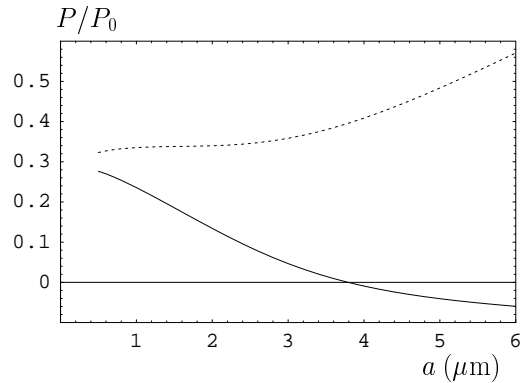


Figure 9. The relative Casimir pressures as functions of separation at $T = 300$ K in the configuration of one plate made of ferromagnetic dielectric and the other plate made of Au with account of magnetic properties (solid line) and with magnetic properties disregarded (dashed line). Computations are performed using the plasma model for the dielectric permittivity of Au.

dielectric permittivity of the used ferromagnetic dielectric can be presented in the form [106]

$$\varepsilon_{\text{fd}}^{(1)}(i\xi) = \varepsilon_d(i\xi) \left(1 + \frac{3f}{1-f} \right). \quad (30)$$

The dielectric permittivity of Au is described by Eq. (17) with $n = 2$, $\omega_p^{(2)} = 9.0$ eV.

The computational results for the relative Casimir pressure P/P_0 at $T = 300$ K as a function of separation are presented in Fig. 9. The solid (dashed) lines show the results obtained with magnetic properties of ferromagnetic plate included (disregarded). As is seen in Fig. 9, there is the profound effect of magnetic properties of ferromagnetic dielectric on the Casimir pressure. Thus, at separations of 0.5, 2, and 6 μm the values of $\eta_{P,\text{fd-Au}}^p$ are equal to -14% , -60% , and -110% , respectively. What is more important, the Casimir pressure P (and, thus, the Casimir force acting between parallel plates through a vacuum gap) changes sign and becomes positive at separations $a > 3.8 \mu\text{m}$. This means that the Casimir force becomes repulsive if Au plate is described by the plasma model. The effect of repulsion between a nonmagnetic metal plate and a ferromagnetic dielectric plate can be used as an experimental test for the influence of magnetic properties on the Casimir force and for the model of dielectric permittivity of a metal plate.

As was mentioned in the beginning of this section, at the Curie temperature T_C specific for each material, ferromagnets undergo a phase transition [107]. At higher temperature they become paramagnets with negligibly small magnetic properties with respect to the Casimir force. The Curie temperature varies over a wide temperature region (for Co, for instance, it is equal to 1388 K). Keeping in mind to investigate the behavior of the Casimir pressure under the magnetic phase transition, it is preferable to deal with two plates made of ferromagnetic metal possessing the Curie temperature close to room temperature, such as Gd (T_C is of about 290 K). Dielectric properties of Gd are described by either the Drude or the plasma model with the parameters [108] $\omega_{p,\text{Gd}} = 9.1$ eV and $\gamma_{\text{Gd}} = 0.58$ eV. The dependence of static magnetic permeability of Gd as a function of temperature in the vicinity of Curie temperature is modeled in Fig. 10(a) using the data of Ref. [109].

Computations of the relative Casimir pressure P/P_0 in the configuration of two Gd plates were performed at $a = 500$ nm as a function of temperature using Eq. (1). The computational results are presented in Fig. 10(b), where the pairs of solid and dashed lines marked 1 and 2 indicate the results computed using the Drude and plasma models, respectively. As before, the solid lines take into account and the dashed lines disregard the magnetic properties of Gd. As can

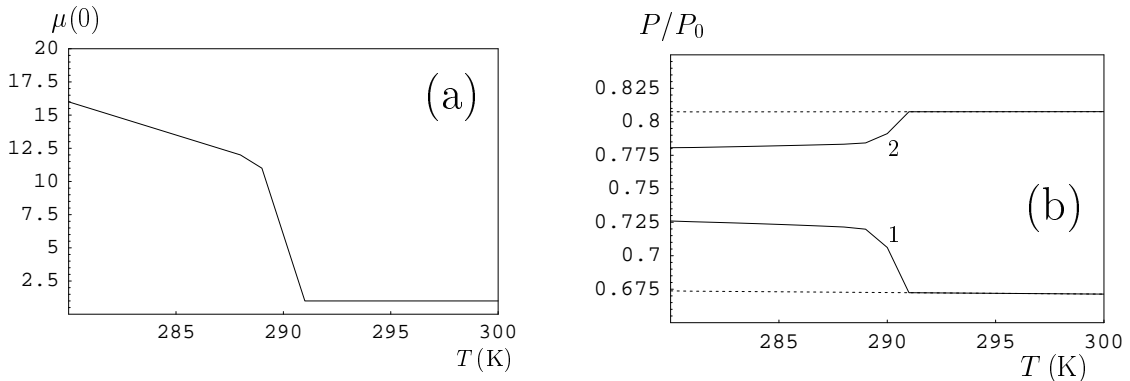


Figure 10. (a) The static magnetic permeability of Gd in the magnetic phase transition as a function of temperature. (b) The relative Casimir pressures as functions of temperature in the configuration of two parallel Gd plates at the separation $a = 0.5 \mu\text{m}$. The solid and dashed lines take into account and disregard the magnetic properties, respectively. The pairs of lines marked 1 and 2 indicate respective computational results obtained using the Drude and plasma models.

be seen in Fig. 10(b), at $T > T_C$ the magnetic properties do not influence the Casimir pressure, whereas the Drude and plasma model approaches lead to results differing for about -19.5% . At $T < T_C$ the magnetic properties influence the Casimir pressure. Quantitatively, at $T = 280$ K the relative influence of magnetic properties on the Casimir pressure is $\eta_{P,\text{Gd}}^D = 7.4\%$ for the Drude model and $\eta_{P,\text{Gd}}^p = -3.3\%$ for the plasma model. With account of magnetic properties, the relative difference between the predictions of the Drude and plasma model approaches for the Casimir pressure is approximately equal to -7% . Thus, the magnetic phase transition provides additional opportunities for the investigation of the impact of magnetic properties on the Casimir force and for the selection between different models of dielectric permittivity.

To conclude this section, we note that possible influence of magnetic properties of ferromagnets on the Casimir force may be considered as somewhat analogous to the influence of real drift current of conduction electrons discussed in Sec. 2. If it is assumed that the fluctuating electromagnetic field can initiate such a current, we arrive at the Drude model approach to the thermal Casimir force which is considered as most natural by some authors [41, 42, 43]. This approach, however, was found to be in contradiction with the results of several experiments [9, 10, 11, 12, 13, 14, 15, 16]. In this connection the problem arises whether the fluctuating electromagnetic field can lead to magnetic effects in ferromagnets which remains to be solved.

5. Lateral Casimir force at the nanoscale

The most universally known *normal* Casimir force acts in the direction perpendicular to the interacting surfaces. However, when the material surfaces of the interacting bodies are anisotropic or they are positioned asymmetrically, a lateral Casimir force may exist, which acts tangential to the surface [17]. Experimentally the lateral Casimir force was first measured [18, 19] in the configuration of a sinusoidally corrugated Au-coated sphere above a sinusoidally corrugated Au-coated plate with equal corrugation periods. The measurement data were compared with theoretical predictions using the PFA. For two parallel ideal metal plates covered with uniaxial sinusoidal corrugations of equal periods the lateral Casimir force was calculated using the exact theory in the second perturbation order with respect to relative corrugation amplitude [110]. For sinusoidally corrugated plates made of real metals described by the plasma model, the lateral Casimir force was calculated in Refs. [111, 112] also in the second-order perturbation theory. Experimentally, the lateral Casimir force becomes measurable only for

sufficiently large amplitudes of corrugations and at sufficiently short separations. Because of this, calculational methods restricted by the second-order perturbation theory are usually not sufficient for the comparison with the measurement data [113].

In the first measurement of the lateral Casimir force [18, 19] the corrugation amplitudes were $A_1 = 59$ nm on the plate and $A_2 = 8$ nm on the sphere. The period of corrugations was equal to $\Lambda = 1200$ nm, i.e., much larger than the separation between the sphere and the plate. The lateral Casimir force with an amplitude of 3.2×10^{-13} N at the shortest separation was found to sinusoidally oscillate as a function of the phase shift φ between the corrugations. It was also predicted theoretically, but not observed experimentally due to the use of insufficiently large corrugation amplitudes, that the lateral Casimir force is in fact asymmetric, i.e., deviates from purely sinusoidal harmonic dependence on the phase shift (this phenomenon is absent when computations are performed up to the second perturbation order).

In the recently performed new measurements of the lateral Casimir force between the Au-coated sphere and plate covered with uniaxial sinusoidal corrugations, the corrugation amplitudes were $A_1 = 85.4$ nm on the plate and $A_2 = 13.7$ nm on the sphere ($\tilde{A}_2 = 25.5$ nm in the second set of measurements). The corrugations had an average period $\Lambda = 574.7$ nm, i.e., more than two times smaller than in Refs. [18, 19] in order to achieve the regime where the PFA becomes inapplicable to the calculation of the lateral Casimir force [see Fig. 11(a,b) where the corrugated surfaces of the plate and of the sphere used in the first set of measurements, respectively, are shown]. To obtain corrugations on the sphere with exactly the same period, as on the plate, a homogeneous sphere was sandwiched against the plate and pressed by means of a piezo. In such a manner sinusoidal corrugations from the plate were imprinted on the sphere. This was done preserving the sphericity of a sphere (see Fig. 12, where the lighter tone shows higher points on the surface of the sphere used in the first set of measurements).

Taking into account the sphericity of the second body and sinusoidal corrugations on both bodies in the framework of the PFA and using the Lifshitz formula (1), one arrives to the following approximate expression for the lateral Casimir force [21]

$$F_{\text{lat}}(a, T, \varphi) = \frac{\pi k_B T R A_1 A_2}{2a^3 \Lambda \beta} \sin \varphi \sum_{n=1}^{\infty} \int_{\zeta_l}^{\infty} y dy e^{-ny} I_1(n\beta y) \left[r_{\text{TM}}^{2n}(i\zeta_l, y) + r_{\text{TE}}^{2n}(i\zeta_l, y) \right]. \quad (31)$$

Here,

$$\beta \equiv \beta(a, \varphi) = \frac{1}{a} (A_1^2 + A_2^2 - 2A_1 A_2 \cos \varphi)^{1/2}, \quad (32)$$

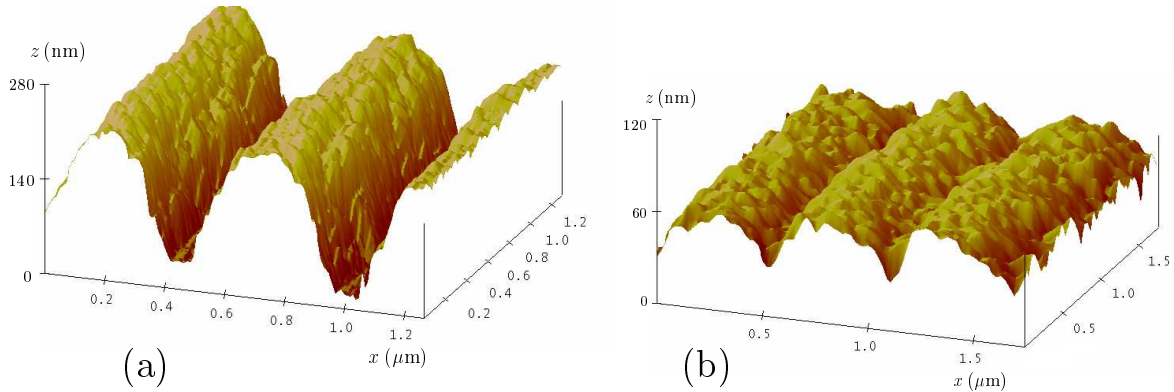


Figure 11. An AFM scan (a) of the plate surface and (b) of the surface of the sphere showing the sinusoidal corrugations covered with stochastic roughness.

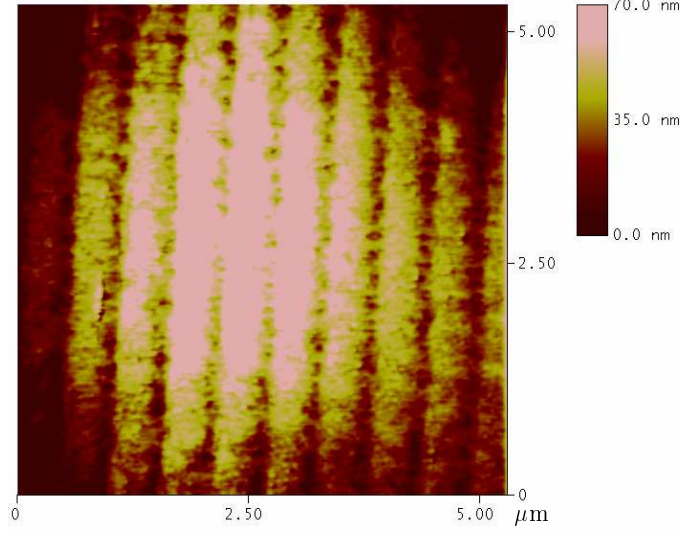


Figure 12. The imprinted corrugations on the sphere. The lighter area shows higher points and hence demonstrates the sphericity of the imprinted surface.

$I_1(z)$ is the Bessel function of an imaginary argument, and the following dimensionless variables are used:

$$y = 2aq_l, \quad \zeta_l = \frac{2a\xi_l}{c}. \quad (33)$$

Remembering that Eq. (31) uses the PFA for the description of sinusoidal corrugations, it should lead to sufficiently exact results under a condition $2\pi a \ll \Lambda$ [6, 8]. As to the applicability of the PFA to sphere-plate geometry, this is guaranteed with large safety margin because $a \ll R = 97 \mu\text{m}$.

Measurements of the lateral Casimir force in Refs. [20, 21] were performed at separations between the mean levels of corrugations of about 100–200 nm. Because of this, the application condition of the PFA for the description of corrugations was not satisfied. Therefore, some corrections to Eq. (31) due to diffraction-type effects were expected to arise. To take the diffraction-type effects into account, the exact description of corrugations using the Rayleigh scattering theory was developed [20, 21] while preserving the use of the PFA for the description of sphere-plate geometry, where it is sufficiently accurate. As a result, the following “exact” expression for the lateral Casimir force was obtained [20, 21]

$$F_{\text{lat}}^{\text{exact}}(a, T, \varphi) = \frac{4k_B T R}{\Lambda} \int_a^\infty dz \sum_{l=0}^{\infty} \frac{\partial}{\partial \varphi} \int_0^\infty dk_y \int_0^{\pi/\Lambda} dk_x \quad (34)$$

$$\times \ln \det \left[I - R_{\text{bot}}^{(1)}(\mathbf{k}_\perp, i\xi_l) R_{\text{top}}^{(2)}(\mathbf{k}_\perp, i\xi_l, z + A_1 + A_2, \varphi) \right].$$

Here, $R_{\text{bot}}^{(1)}$ ($R_{\text{top}}^{(2)}$) is the reflection matrix of the downward (upward) moving waves on the bottom (top) grating under a condition that the top (bottom) grating is removed, and I is an infinite dimensional unit matrix. In both Eqs. (31) and (34) the dielectric properties of Au were taken into account by means of the generalized plasma-like model (24).

In Fig. 13(a) we show the measured data in the first set of measurements (dots) and computed using the exact theory of Eq. (34) lateral Casimir force (solid line) over four corrugation periods versus the normalized lateral displacement x/Λ between the corrugated surfaces at a separation

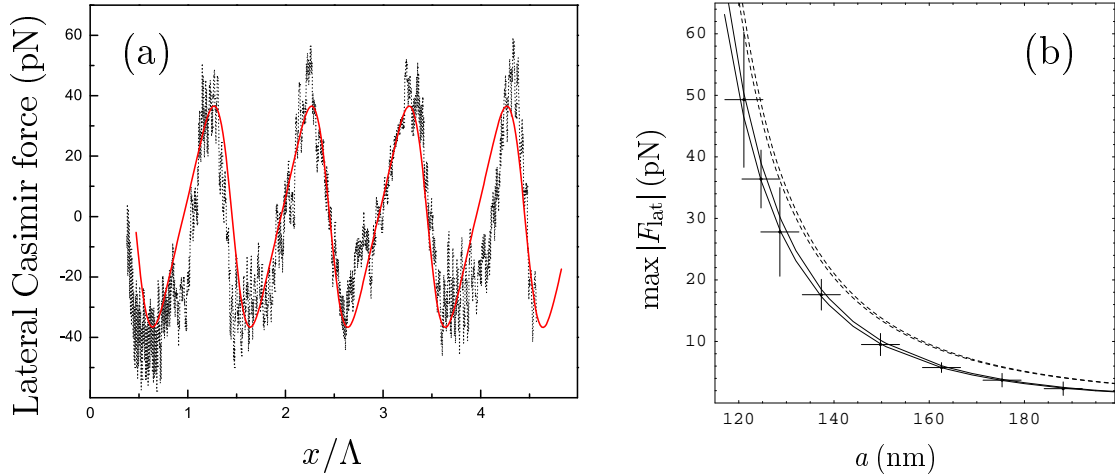


Figure 13. (a) The experiment (dots) and the exact theory (solid line) for the lateral Casimir force versus the lateral displacement normalized for the corrugation period at the separation 124.7 nm. No fitting parameters are used. (b) The experimental data (crosses) and theoretical values computed using the exact theory (the band between the solid lines) and using the proximity force approximation (the band between the dashed lines) for the maximum magnitudes of the lateral Casimir force versus separation. No fitting parameters are used.

$a = 124.7$ nm (similar figures related to larger separations and to the second set of measurements can be found in Ref. [21]). As can be seen in Fig. 13(a), the lateral Casimir force is a periodic function of the phase shift. The important characteristic feature of the periodic curve shown in the figure is that it is *asymmetric*, i.e., the dependence of F_{lat} on x/Λ is not strictly sinusoidal (note that the sinusoidal dependence of the lateral force on $\varphi = 2\pi x/\Lambda$ holds only if the calculations are restricted to the second order in corrugation amplitudes $\sim A_1 A_2$). The true asymmetry of the measured lateral force is obvious even without the theory line. For example, in Fig. 13(a) the average shift of each maximum point from the midpoint of two adjacent minima is $(0.12 \pm 0.01)\Lambda$. We emphasize that the theoretical solid line was obtained with no fitting parameters. As can be seen in Fig. 13(a), the exact theory of Eq. (34) is in a very good agreement with the experimental data shown as dots.

The experimental data for the $\max |F_{\text{lat}}|$ versus separation a are shown in Fig. 13(b) as crosses. The arms of crosses indicate the total experimental error determined at a 95% confidence level for each experimental point individually. The exact computational results for the $\max |F_{\text{lat}}|$ are shown in Fig. 13(b) as a band between the two solid lines versus separation. The width of this band takes into account the computational errors and the correction to Eq. (34) due to surface roughness. As is seen in Fig. 13(b), the exact theory is in a very good agreement with the measurement data. The computational results for the $\max |F_{\text{lat}}|$ at different separations obtained using the PFA [Eq. (31)] are shown in Fig. 13(b) as a band between two dashed lines. The width of this band takes into account the role of surface roughness. As can be seen in Fig. 13(b), the experimental data indicated as crosses are inconsistent with the prediction of the PFA approach, thus revealing the role of diffraction-type effects for corrugations of relatively small period used in this experiment.

Besides fundamental interest in the phenomenon of lateral Casimir force as one more manifestation of the zero-point oscillations of electromagnetic field, it is pertinent to note that this version of the Casimir force gives the possibility to actuate lateral translations of corrugated surfaces in micromachines. The lateral Casimir force might be used to solve the tribological problems plaguing the microdevice industry. Specifically, it was proposed to use this effect

for the frictionless transmission of lateral motion by means of a nanoscale rack and pinion without intermeshing cogs [114, 115, 116] or in a ratchet with asymmetric corrugations driven by the Casimir force [117]. Such devices could be used for transferring motion between two microelectromechanical systems without mechanical contact. The experimental and theoretical results on the lateral Casimir force discussed above bring us closer to the realization of micromachines driven by the zero-point fluctuations of quantum vacuum.

6. Conclusions and discussion

In the foregoing, we have listed several experiments and theoretical advances in the Casimir effect which has come to the center of public attention very recently. The Casimir effect deals with quantum vacuum, which is the most fundamental and puzzling type of physical reality. This is a possible reason why the research area in this field is so wide. On the one hand, it is closely connected with foundations of quantum statistical physics and even calls for reconsideration of some of its basic concepts. On the other hand, the Casimir effect quickly turns into a practical tool of nanotechnology which is expected to find numerous applications in the next generation of microdevices.

As was discussed in Sec. 2, the fundamental Lifshitz theory of the van der Waals and Casimir forces comes into conflict with basics of thermodynamics when the relaxation properties of free charge carriers are taken into account. In Sec. 3, the three landmark recently performed experiments are described demonstrating that in a literal sense, the Lifshitz theory is in a deep contradiction with the measurement data. Only if we accept the phenomenological prescription that for dielectrics charge carriers are disregarded and for metals they are described by the plasma model, the theoretical predictions of the Lifshitz theory come in agreement with the data. This situation cannot be considered as satisfactory. In fact we deal with some kind of a paradox. The mathematical formalism of the Lifshitz theory during the last few years has undergone far reaching generalization discussed in Secs. 2 and 5. It is presently possible to write the Lifshitz-type formulas for compact objects of arbitrary shape in terms of reflection amplitudes of electromagnetic oscillations on their surfaces. Based on this it was even believed that at the present time computation of the Casimir force between any bodies is only a problem of sufficient computer facilities. As was argued in Secs. 2 and 3, the problem is, however, much deeper. In fact the reflection amplitudes suggested by our knowledge of physical processes with real (not fluctuating) electromagnetic fields lead to computational results in contradiction with the experimental data making powerful mathematical formalism at least insufficient. This is a fundamental problem to be solved in the future.

From the point of view of applications in nanotechnology, large progress on the control the magnitude of the Casimir force was achieved. This was done by means of a modification of dielectric properties by using different materials and different influential factors such as irradiation with laser light. In several experiments considered in Sec. 4.1 it was possible to modify the magnitude of the Casimir force from a few percent to about 50%. There were several proposals on how to achieve the Casimir repulsion through the vacuum gap, but to the present day the Casimir repulsion was realized only in the familiar three-layer system. One more opportunity to control the magnitude of the Casimir force is suggested by phase transitions. In Sec. 4.1 we have discussed the phase transition from dielectric to the metallic state. A few tens of percent variation in the magnitude of the Casimir force is achievable under a phase transition of the plate material.

Quick progress in the application of the Casimir force in nanotechnology might be caused by the use of ferromagnetic materials. For real material properties this subject was investigated only recently (see Sec. 4.2). What is most striking, according to the Lifshitz theory the Casimir interaction of a nonmagnetic metallic plate described by the plasma model with a ferromagnetic dielectric plate through the vacuum gap becomes repulsive under some conditions. This effect,

if exists in nature, opens up the way for the developments of various microdevices. We should notice, however, that the influence of magnetic properties on the Casimir interaction is not yet confirmed experimentally. The confirmation or exclusion of such an influence is expected in the near future.

One more opportunity for applications in nanotechnology is suggested by the lateral Casimir force discussed in Sec. 5. Together with the normal Casimir force, it gives the possibility to actuate both normal and lateral translations of corrugated surfaces in micromachines by means of the electromagnetic zero-point oscillations. With respect to tribological problems, the lateral Casimir force allows frictionless transition of lateral motion. All the above allows to conclude that the Casimir effect promises important breakthroughs in both fundamental physics and its applications in nanotechnology.

Acknowledgments

The author is grateful to the Organizing Committee of ICSF2010 for the invitation to present this talk, kind hospitality during the Conference and financial support. CNPq (Brazil), process 310039/2010-0 is also acknowledged for partial financial support. I am grateful to all co-authors of joint papers for helpful discussions and collaboration.

- [1] Casimir H B G 1948 *Proc. K. Ned. Akad. Wet.* **51** 793
- [2] Buks E and Roukes M L 2001 *Phys. Rev. B* **63** 033402
- [3] Chan H B, Aksyuk V A, Kleiman R N, Bishop D J and Capasso F 2001 *Science* **291** 1941
- [4] Lifshitz E M 1956 *Zh. Eksp. Teor. Fiz.* **29** 94 (*Sov. Phys. JETP* **2** 73)
- [5] Dzyaloshinskii I E, Lifshitz E M and Pitaevskii L P 1961 *Sov. Phys. Usp.* **4** 153
- [6] Klimchitskaya G L, Mohideen U and Mostepanenko V M 2009 *Rev. Mod. Phys.* **81** 1827
- [7] Mostepanenko V M and Klimchitskaya G L 2010 *Int. J. Mod. Phys. A* **25** 2302
- [8] Bordag M, Klimchitskaya G L, Mohideen U and Mostepanenko V M 2009 *Advances in the Casimir Effect* (Oxford: Oxford University Press)
- [9] Decca R S, Fischbach E, Klimchitskaya G L, Krause D E, López D and Mostepanenko V M 2003 *Phys. Rev. D* **68** 116003
- [10] Decca R S, López D, Fischbach E, Klimchitskaya G L, Krause D E and Mostepanenko V M 2005 *Ann. Phys. NY* **318** 37
- [11] Decca R S, López D, Fischbach E, Klimchitskaya G L, Krause D E and Mostepanenko V M 2007 *Phys. Rev. D* **75** 077101
- [12] Decca R S, López D, Fischbach E, Klimchitskaya G L, Krause D E and Mostepanenko V M 2007 *Eur. Phys. J. C* **51** 963
- [13] Chen F, Klimchitskaya G L, Mostepanenko V M and Mohideen U 2007 *Optics Express* **15** 4823
- [14] Chen F, Klimchitskaya G L, Mostepanenko V M and Mohideen U 2007 *Phys. Rev. B* **76** 035338
- [15] Obrecht J M, Wild R J, Antezza M, Pitaevskii L P, Stringari S and Cornell E A 2007 *Phys. Rev. Lett.* **98** 063201
- [16] Klimchitskaya G L and Mostepanenko V M 2008 *J. Phys. A: Math. Theor.* **41** 312002
- [17] Golestanian R and Kardar M 1997 *Phys. Rev. Lett.* **78** 3421
- [18] Chen F, Mohideen U, Klimchitskaya G L and Mostepanenko V M 2002 *Phys. Rev. Lett.* **88** 101801
- [19] Chen F, Mohideen U, Klimchitskaya G L and Mostepanenko V M 2002 *Phys. Rev. A* **66** 032113
- [20] Chiu H-C, Klimchitskaya G L, Marachevsky V N, Mostepanenko V M and Mohideen U 2009 *Phys. Rev. B* **80** 121402(R)
- [21] Chiu H-C, Klimchitskaya G L, Marachevsky V N, Mostepanenko V M and Mohideen U 2010 *Phys. Rev. B* **81**, 115417
- [22] Bimonte G, Klimchitskaya G L and Mostepanenko V M 2009 *Phys. Rev. A* **79** 042906
- [23] Zhou F and Spruch L 1995 *Phys. Rev. A* **52** 297
- [24] Tomaš M S 2002 *Phys. Rev. A* **66** 052103
- [25] Raabe C, Knöll L and Welsch D-G 2003 *Phys. Rev. A* **68** 033810
- [26] Emig T, Jaffe R L, Kardar M and Scardicchio A 2006 *Phys. Rev. Lett.* **96** 080403
- [27] Bulgac A, Magierski P and Wirzba A 2006 *Phys. Rev. D* **73** 025007
- [28] Kenneth O and Klich I 2006 *Phys. Rev. Lett.* **97** 160401
- [29] Bordag M 2006 *Phys. Rev. D* **73** 125018
- [30] Kenneth O and Klich I 2008 *Phys. Rev. B* **78** 014103
- [31] Bordag M and Pirozhenko I 2010 *Phys. Rev. D* **81** 085023

- [32] Wilson A G 1931 *Proc. Roy. Soc. Lond. A* **133** 458
- [33] Mott N F 1990 *Metal-Insulator Transitions* (London: Taylor and Francis)
- [34] Parsegian V A 2005 *Van der Waals forces: A Handbook for Biologists, Chemists, Engineers, and Physicists* (Cambridge: Cambridge University Press)
- [35] Inui N 2003 *J. Phys. Soc. Jap.* **72** 2198
- [36] Palik E D (ed) 1985 *Handbook of Optical Constants of Solids* (New York: Academic)
- [37] Geyer B, Klimchitskaya G L and Mostepanenko V M 2005 *Phys. Rev. D* **72** 085009
- [38] Klimchitskaya G L and Geyer B 2008 *J. Phys. A.: Mat. Theor.* **41** 164032
- [39] Bezerra V B, Klimchitskaya G L and Mostepanenko V M 2002 *Phys. Rev. A* **66** 062112
- [40] Bezerra V B, Klimchitskaya G L, Mostepanenko V M and Romero C 2004 *Phys. Rev. A* **69** 022119
- [41] Boström M and Sernelius B E 2004 *Physica A* **339** 53
- [42] Høyе J S, Brevik I, Ellingsen S A and Aarseth J B 2007 *Phys. Rev. E* **75** 051127
- [43] Brevik I, Ellingsen S A, Høyе J S and Milton K A 2008 *J. Phys. A: Math. Theor.* **41** 164017
- [44] Klimchitskaya G L and Mostepanenko V M 2008 *Phys. Rev. E* **77** 023101
- [45] Klimchitskaya G L, Mohideen U and Mostepanenko V M 2008 *J. Phys. A: Math. Theor.* **41** 432001
- [46] Pitaevskii L P 2008 *Phys. Rev. Lett.* **101** 163202
- [47] Dalvit D A R and Lamoreaux S K 2008 *Phys. Rev. Lett.* **101** 163203
- [48] Chazalviel J-N 1999 *Coulomb Screening of Mobile Charges: Applications to Material Science, Chemistry and Biology* (Boston: Birkhauser)
- [49] Geyer B, Klimchitskaya G L, Mohideen U and Mostepanenko V M 2009 *Phys. Rev. Lett.* **102** 189301
- [50] Mostepanenko V M, Decca R S, Fischbach E, Geyer B, Klimchitskaya G L, Krause D E, López D and Mohideen U 2009 *Int. J. Mod. Phys. A* **24** 1721
- [51] Klimchitskaya G L 2009 *J. Phys. Conf. Ser.* **161** 012002
- [52] Dure J C, Maass P, Roling B and Sidebottom D L 2009 *Rep. Progr. Phys.* **72** 046501
- [53] Shklovskii B I and Efros A L 1984 *Electronic Properties of Doped Semiconductors. Solid State Series*, v.45 (Berlin: Springer)
- [54] Decca R S, Fischbach E, Geyer B, Klimchitskaya G L, Krause D E, López D, Mohideen U and Mostepanenko V M 2009 *Phys. Rev. Lett.* **102** 189303
- [55] Mostepanenko V M, 2009 *J. Phys. Conf. Ser.* **161** 012003
- [56] Pitaevskii L P 2009 *Phys. Rev. Lett.* **102** 163203
- [57] Dalvit D A R and Lamoreaux S K 2009 *Phys. Rev. Lett.* **102** 163204
- [58] Krause D E, Decca R S, López D and Fischbach E 2007 *Phys. Rev. Lett.* **98** 050403
- [59] Canaguier-Durand A, Maia Neto P A, Lambrecht A and Reynaud S 2010 *Phys. Rev. Lett.* **104** 040403
- [60] Canaguier-Durand A, Maia Neto P A, Lambrecht A and Reynaud S 2010 *Phys. Rev. A* **82** 012511
- [61] Zandi R, Emig T and Mohideen U 2010 *Phys. Rev. B* **81** 195423
- [62] Lambrecht A and Reynaud S 2000 *Eur. Phys. J. D* **8** 309
- [63] Pirozhenko I, Lambrecht A and Svetovoy V B 2006 *New J. Phys.* **8** 238
- [64] Svetovoy V B, van Zwol P J, Palasantzas G and Hosson J Th M 2008 *Phys. Rev. B* **77** 035439
- [65] Decca R S, López D and Osquiguil E 2010 *Int. J. Mod. Phys. A* **25** 2223
- [66] Geyer B, Klimchitskaya G L and Mostepanenko V M 2010 *Phys. Rev. B* **81** 245421
- [67] Inui N 2004 *J. Phys. Soc. Jap.* **73** 332
- [68] Inui N 2006 *J. Phys. Soc. Jap.* **75** 024004
- [69] Inui N 2007 *J. Phys. Conf. Ser.* **89** 012018
- [70] Mostepanenko V M and Geyer B 2008 *J. Phys. A: Mat. Theor.* **41** 164014
- [71] Shapiro B 2010 *Phys. Rev. B* **82** 075205
- [72] Antezza M, Pitaevskii L P and Stringari S 2004 *Phys. Rev. A* **70** 053619
- [73] Antezza M, Pitaevskii L P and Stringari S 2005 *Phys. Rev. Lett.* **95** 113202
- [74] Harber D M, Obrecht J M, McGuirk J M and Cornell E A 2005 *Phys. Rev. A* **72** 033610
- [75] Caride A O, Klimchitskaya G L, Mostepanenko V M and Zanette S I 2005 *Phys. Rev. A* **71** 042901
- [76] Silveirinha M G 2010 *Phys. Rev. B* **82** 085101
- [77] Chen F, Mohideen U, Klimchitskaya G L and Mostepanenko V M 2005 *Phys. Rev. A* **72** 020101(R)
- [78] Chen F, Mohideen U, Klimchitskaya G L and Mostepanenko V M 2006 *Phys. Rev. A* **74** 022103
- [79] Chen F, Klimchitskaya G L, Mostepanenko V M and Mohideen U 2006 *Phys. Rev. Lett.* **97** 170402
- [80] deMan S, Heeck K, Wijngaarden R J and Iannuzzi D 2009 *Phys. Rev. Lett.* **103** 040402
- [81] Milling A, Mulvaney P and Larson I 1996 *J. Colloid Interface Sci.* **180** 460
- [82] Meurk A, Luckham P F and Bergström L 1997 *Langmuir* **13** 3896
- [83] Lee S-W and Sigmund M W 2002 *Colloids Surf. A* **204** 43
- [84] Munday J N, Capasso F and Parsegian V A 2009 *Nature* **457** 170
- [85] Geyer B, Klimchitskaya G L, Mohideen U and Mostepanenko V M 2008 *Phys. Rev. A* **77** 036102

- [86] van Zwol P J, Palasantzas G and Hosson J Th M 2009 *Phys. Rev. B* **79** 195428
- [87] Klimchitskaya G L, Mohideen U and Mostepanenko V M 2007 *J. Phys. A.: Mat. Theor.* **40** F841
- [88] Mostepanenko V M and Trunov N N 1997 *The Casimir Effect and Its Applications* (Oxford: Oxford University Press)
- [89] Bimonte G, Calloni E, Exposito G, Milano L and Rosa L 2005 *Phys. Rev. Lett.* **94** 180402
- [90] Bimonte G, Calloni E, Exposito G and Rosa L 2005 *Nucl. Phys. B* **726** 441
- [91] Bimonte G 2008 *Phys. Rev. A* **78** 062101
- [92] Castillo-Garza R, Chang C-C, Jimenez D, Klimchitskaya G L, Mostepanenko V M and Mohideen U 2007 *Phys. Rev. A* **75** 062114
- [93] Pirozhenko I and Lambrecht A 2008 *Phys. Rev. A* **77** 013811
- [94] Torricelli G, van Zwol P J, Shpak O, Binus C, Palasantzas G, Kooi B J, Svetovoy V B and Wuttig M 2010 *Phys. Rev. A* **82** 010101(R)
- [95] Kenneth O, Klich I, Mann A and Revzen M 2002 *Phys. Rev. Lett.* **89** 033001
- [96] Iannuzzi D and Capasso F 2003 *Phys. Rev. Lett.* **91** 029101
- [97] Vonsovskii S V 1974 *Magnetism* (New York: J. Wiley).
- [98] Geyer B, Klimchitskaya G L and Mostepanenko V M 2010 *Phys. Rev. B* **81** 104101
- [99] Klimchitskaya G L, Geyer B and Mostepanenko V M 2010 *Int. J. Mod. Phys. A* **25** 229360
- [100] Rahi S J, Emig T, Graham N, Jaffe R L and Kardar M 2009 *Phys. Rev. D* **80** 085021
- [101] Tomaš M S 2005 *Phys. Lett. A* **342** 381
- [102] Goldman A 1999 *Handbook of Modern Ferromagnetic Materials* (New York: Springer)
- [103] Ordal M A, Bell R J, Alexander Jr R W, Long LL and Querry M R 1985 *Appl. Opt.* **24** 4493
- [104] Chambers S A 2006 *Surf. Sci. Rep.* **61** 345
- [105] Roy K and Datta A N 1974 *J. Phys. D* **7** 1053
- [106] Lewin L 1947 *J. Inst. Electr. Eng. Part 3* **94** 64
- [107] Ausloos M (ed) 1983 *Magnetic Phase Transitions* (New York: Springer)
- [108] Palik E D (ed) 1998 *Handbook of Optical Constants of Solids III* (New York: Academic)
- [109] Coey J M D, Skumryev V and Gallagher K 1999 *Nature* **401** 35
- [110] Emig T, Hanke A, Golestanian R and Kardar M 2003 *Phys. Rev. A* **67** 022114
- [111] Rodrigues R B, Maia Neto P A, Lambrecht A and Reynaud S 2006 *Phys. Rev. Lett.* **96** 100402
- [112] Rodrigues R B, Maia Neto P A, Lambrecht A and Reynaud S 2006 *Phys. Rev. A* **75** 062108
- [113] Chen F, Mohideen U, Klimchitskaya G L and Mostepanenko V M 2006 *Phys. Rev. Lett.* **98** 068901
- [114] Ashourvan A, Miri M and Golestanian R 2007 *Phys. Rev. Lett.* **98** 140801
- [115] Ashourvan A, Miri M and Golestanian R 2007 *Phys. Rev. E* **75** 040103(R)
- [116] Ashourvan A, Miri M and Golestanian R 2007 *J. Phys. Conf. Ser.* **89** 012017
- [117] Emig T 2007 *Phys. Rev. Lett.* **98** 160801